2011

Self-Alignment of Silicon Microparts on a Hexadecane-Water Interface by Surface Tension

Caroline Elizabeth Liberti
University of South Florida, cliberti@mail.usf.edu

Self-Alignment of Silicon Microparts on a Hexadecane-Water Interface by Surface Tension

by

Caroline E. Liberti

A thesis submitted in partial fulfillment
of the requirements for the degree of
Master of Science in Mechanical Engineering
Department of Mechanical Engineering
College of Engineering
University of South Florida

Major Professor: Nathan Crane, Ph.D.
Nathan Gallant, Ph.D.
Rasim Guldiken, Ph.D.

Date of Approval:
June 9, 2011

Keywords: Micro Self-Assembly, Lateral Capillary Forces, Fluid-Fluid Interface, Hexadecane, Microchip

Acknowledgements

This work was completed in part through funding provided by Sandia National Laboratories and with the assistance of Jose Carballo, Ph.D. candidate and Nathan Crane, Ph.D.

Table of Contents

List of Tables

List of Figures

Abstract

Mechanical assembly of systems and structures on the micro-scale can be inefficient as particles of sub-millimeter dimensions are difficult to manipulate. Cutting edge manufacturing methods implement self-assembly as an approach to ordering micro and nano-sized parts into a desired arrangement. This thesis studies a technique utilizing surface tension as a method of actuating microparts on a liquid-liquid interface via lateral capillary interactions. Preliminary experimentation is conducted to investigate the feasibility of developing a new method for self-alignment of microparts by observing the influence of interfacial geometry on the movement of silicon tiles along a hexadecane-water interface. Different surface geometries are created by implementing vertical rods of different wetting properties that alter the curvature of the interface. Results demonstrate that the microparts attain an equilibrium separation distance from the vertical rods. It is indicated that this equilibrium distance is determined by the dimensions of the micropart and the curvature of the interface. With further investigation, these results may be used to cultivate a method for self-alignment of microparts into rings of a desired radius.

Chapter 1:

Introduction

This thesis explores the prospect of developing an innovative method of self-assembly on the micro-scale by investigating the behavior of micro-scale parts on a liquid-liquid interface. The data collected by studying the movement that microparts exhibit on a curved interface provides valuable insights into feasible structures and methods for assembly of micro-scale parts at a liquid-liquid interface.

Previous research in the area of manipulation of micro and nanoparts on a fluid-fluid interface investigated the capillary forces that emerge along the interfacial plane between floating bodies. The presence of a body on the surface of a fluid deforms the flat surface by creating either a concave or a convex meniscus surrounding the particle. This deformation effect is driven by gravity and the shape of the fluid becomes dependent on the weight of the floating particle. Two similar particles that deform the surface of the liquid in the same direction will exhibit a lateral attraction to one another [1]. Two particles that cause opposite directions of surface deformation experience repulsion [1].

Some previous work demonstrates the attraction and repulsion effect by capillary forces between two bodies that are semi-immersed in a fluid as opposed to floating on the surface. A semi-immersed body is a fixed body that is supported in a fluid bath and is only partially immersed in the fluid so that the top of the solid protrudes up through the interface [1]. The deformation of a fluid surface by an immersed body is dependent upon

the wetting characteristics of the body. Other studies implement the use of an electric field in conjunction with lateral capillary forces to enhance the attractive and repulsive forces between bodies [2-7]. Generally, spherical floating or spherical semi-immersed bodies are examined to represent colloidal effects on a liquid-air interface.

An alternative approach is demonstrated in this thesis by studying the ability to manipulate thin, square, silicon floating microparts on a liquid-liquid interface by introducing immersed vertical rods near the microparts. With this method, both floating particles *and* semi-immersed bodies will be present. The shape and material of the microparts represent components that can be used in a wide range of cutting-edge technologies including electronic devices and micro-scale solar cells [8]. The interface is a hexadecane-water interface and is unique to most previous work in surface tension self-assembly.

The effect of lateral capillary forces is observed as it occurs between floating bodies and fixed, semi-immersed bodies as seen in Figure 1.1.

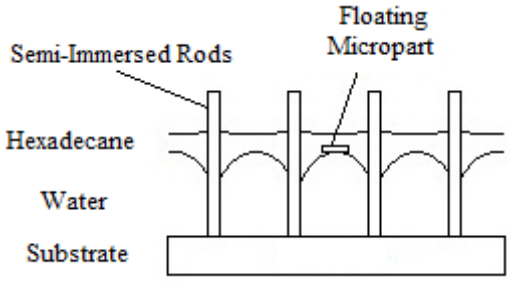

Figure 1.1: Side view of experimental set-up. Set-up includes semi-immersed vertical rods, micropart and hexadecane-water interface.

The direction of movement of the microparts on the interface is determined by the deformation of the interface while the characteristics of the two types of bodies influence this surface deformation. The thesis focuses mainly on the cases where the curvature

changes due to the presence of the semi-immersed bodies are greater than changes made by the floating microparts. The approach described here combines the effects of both lateral flotation capillary forces and lateral immersion capillary forces while considering both gravity on the floating micropart and the wettability of the semi-immersed vertical rods. An experimental demonstration is implemented. Different spacing arrangements and different wetting characteristics of the vertical semi-immersed rods are tested. The effect of the presence of the rods on the lateral motion of the micropart is observed.

The behavioral observations of the floating microparts are analyzed and the impact of the results on the manipulation and positioning of microparts on a liquid-liquid interface is discussed.

1.1 Fundamentals of Self-Assembly

Self-assembly is the term used to describe the process of disordered components self-organizing into an ordered system or array [9]. Design for self-assembly manipulates existing interactions between components to form a desired structure. Mechanical assembly of systems and structures ordinarily requires the method of pick-and-place assembly, which is comprised of individually picking up parts and placing them into alignment to complete an assembly. On the micro and nano-scale, the pick-and-place method is inefficient and costly and micromanipulators have complex structures and can be hard to use [2]. The act of manipulating tiny components can be extremely time-consuming and placement of microparts into an exact location may be difficult. An alternative method in fabrication of small devices, i.e. micro electromechanical systems (MEMS), microchips, etc. is a self-assembly technique that functions with precision and allows for proper alignment of microparts [10]. Currently, the methods of self-assembly

utilize the natural attractive forces that occur between parts such as surface tension, electrostatic forces, magnetic forces and van der Waals forces [9-11].

An understanding of the interactions between parts on the micro-scale is critical for optimal utilization of these forces. When designing for self-assembly, it is recognized that the physical characteristics of individual components determine the nature of the interactions between them. Designing a system to self-assemble involves making use of these natural interactions by choosing the components and the environment where individual mobile parts will interact in a way that produces a desired result, i.e. an ordered structure [9].

Molecular interactions occur at surfaces, across interfaces and between components. They become significant forces in small devices and can influence the behaviors of individual parts and systems as a whole [10]. Selecting the appropriate interactions and adjusting forces allow mobile parts to align. As individual components move in relation to each other due to these physical interactions between them, they can be manipulated to arrange into a pre-designed pattern.

As technology advances and continues to take advantage of a decreasing size scale, it becomes necessary to eliminate or reduce human interaction during assembly [11]. The manufacturing process for tiny systems is increasingly reliant on robotics for assembly. As miniaturization in technology continues, micro and nano fabrication of parts by manipulation by robots becomes difficult and uneconomical [9, 11]. It then becomes necessary to design for self-assembly on the micro-scale and below.

Some of the most abundant examples of self-assembly in nature are DNA replication, protein creation and mitosis of living cells. Engineers can study what is

already successful in biological systems and attempt to replicate and apply it to devices on the nano and micro scale. Understanding self-assembly in nature can lead to the design of self-assembly in manmade mechanisms where other fabrication processes are limiting [11].

1.2 Significance of Surface Tension in Self-Assembly

On the macro-scale, gravity is the dominating force affecting the physics and shape of a body. Gravitational force is a function of the gravitational constant which scales with dimension cubed. Surface tension forces, however, are directly proportional to dimension [12]. Therefore, as the size of a body is reduced, there is ultimately a size in which surface tension forces are a dominating physical contribution to shape and behavior [12]. On the micro-scale, surface tension forces are powerful.

There are an unlimited number of applications of micro technology that motivate a study of self-assembly. Currently, self-assembly by surface tension is researched for applications in the manufacturing of optical devices, bio-electronic devices, sensors, radio frequency identification technologies and several microelectronic devices [3-5, 13]. In the medical industry, surface tension is studied to develop encapsulation of food and drugs by colloids to then be administered into the body [6]. Capillary forces are integral in assisting rapid diagnosis of disease causing agents in immunoassays and in lab-on-a-chip biochemical analysis [4]. Studying surface tension driven self-assembly methods allows for improvement in manufacturing, increase in assembly efficiency, decrease in costs associated with fabrication and increase in performance of such devices.

A promising application for a self-assembled array of silicon tiles exists in solar cells. Crystalline-silicon is the material used in photovoltaic energy systems due to its

reliability and suitable cost [14]. As photovoltaics emerge as a competing resource for producing electrical energy many advancements in solar cell technology is necessary, including large-scale manufacturing [6]. Creating a method for self-assembly of silicon tiles into a micro-scaled array by way of surface tension could lead to the development of a process for wide scale manufacture of micro-photovoltaic cells.

1.3 Thesis Outline

The study of the effects of surface tension on 250 micron, 500 micron and 1 mm wide silicon tiles by implementation of semi-immersed rods on a liquid-liquid interface is explored in this document. The implications of the experimental data on self-assembly are discussed.

Chapter 1 of this thesis introduces the motivation behind the study of surface tension on the micro-scale. The second chapter discusses the background information for the research including relevant equations and previous research that has been conducted in this area.

Chapter 3 presents a model, created in Surface Evolver, used to simulate a fluid surface as it is deformed by vertical rods and a horizontal micropart. The model is used to demonstrate the geometry of the interface and serves as a preliminary step that could lead to future calculations of lateral capillary forces and surface energies.

Chapter 4 describes the development and execution of the physical experiment. The experiment aims to observe the behavior of the microparts as they react to surface tension created by the presence of the vertical rods on the liquid-liquid interface. Chapter 5 reports the results of the experiments.

The final chapter, Chapter 6, discusses the conclusion of the thesis and comments on future work to be done in continuation of research in this area of study. Application for development of a repeatable self-assembly process is also reviewed.

Chapter 2:

Background

2.1 Surface Tension and Capillarity

Capillary forces emerge from surface tension. Surface tension is created as molecules at the surface of a liquid have more energy than molecules beneath the surface. Like molecules of a liquid phase are attracted to each other. Molecules are less densely populated at the surface of a liquid than they are deep within a liquid, causing molecules at the surface to have slightly greater spacing between them [15]. The like molecules at the surface of a liquid maintain cohesion due to their attraction, but with greater attractive forces than there are deep within the liquid. This results in tension at the surface of a liquid which can be utilized in self-assembly to align microparts into a desired position.

Free liquids form an interface with an adjoining liquid or gas. When a liquid interface intersects with a solid surface, like in the instance of a droplet of water sitting on a flat glass plate, a contact angle, θ_c, appears [15]. The contact angle describes the angle between the contact line, shown in Figure 2.1 below, and the solid-water surface. If the contact angle is less than 90º, the surface of the water droplet on the glass is in a lower energy state than the water-air interface. In this case, the glass surface is said to be hydrophilic and the water is wetting. If the contact angle is greater than 90º, the solid-water has more energy than the water-air interface. As a result, the glass surface is said to be hydrophobic and the water is non-wetting. This is demonstrated in Figure 2.2.

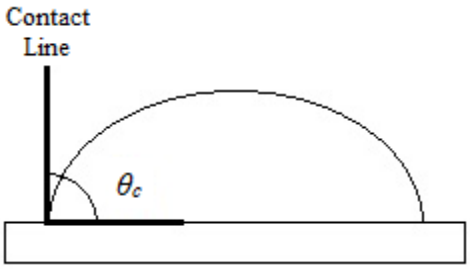

Figure 2.2: Contact angle, θ_c = 90º, for a droplet of water on a glass surface.

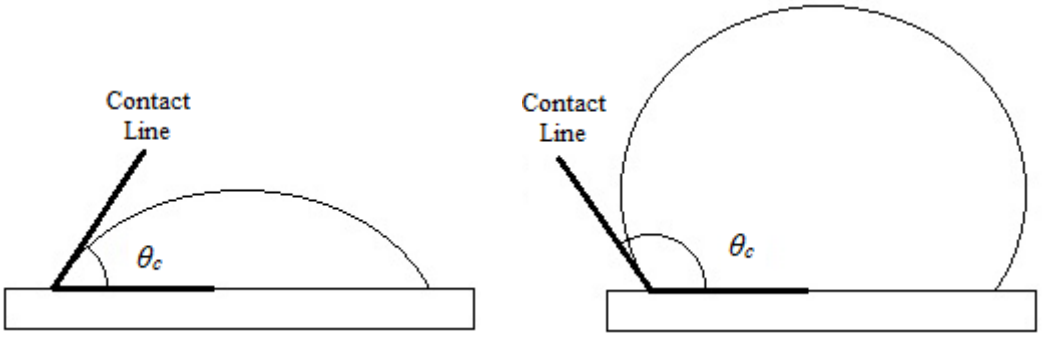

(a) **(b)**

Figure 2.3: Acute and obtuse contact angles. (a) θ_c < 90º, hydrophilic surface, water is wetting, and (b) θ_c > 90º, hydrophobic surface, water is non-wetting.

Forces at the surface of a fluid may be characterized by Laplace's and Young's equations. The theory of capillarity is based on these equations [1]. The Laplace equation is derived from a force balance per unit area of the curved interface of a fluid. Young's equation is formulated from a force balance per unit length at the curved interface. Both force balances include surface tension and contact angle. As mentioned, the contact line describes where three intersecting surfaces meet, depicts the contact angle and it acts tangent to the fluid-fluid interface.

Tension exists at a fluid surface where there is excess energy. The surface tension and contact angle are sensitive to the physicochemical state of the solid-liquid surface[15]. All else being equal, as the contact angle increases, the surface tension effect increases along the fluid-fluid interface in Young's Equation. Both the Laplace and

Young equations neglect any interfacial bending moment and curvature elastic moduli [1].

2.1.1 The Laplace Equation of Capillarity

Several forms of the Laplace equation exist based on the geometry of the fluid surface from which the equation is derived. The forms of the Laplace equation presented here are applicable to fluid-fluid interfaces experimentally demonstrated in this thesis. Surface tension is represented by sigma (σ) and has units of force per length.

2.1.1.1 Laplace Equation of Capillarity for a Spherical Interface

The spherical interface shown in Figure 2.3 depicts the forces present on the curved surface of either a gas or liquid. A fluid-fluid interface assumes a smooth shape when in tension. The curvature created by this shape results in a greater area of the surface. This creates a higher level of energy in the surface. Because of the surface tension present, an inner and outer pressure develops on both sides of the interface. Forces at the interface may be represented in terms of these pressures. The inner and outer pressures at the spherical interface shown are defined as P_1 and P_2, respectively. The radius of the spherical surface of tension, σ, is defined as R, and θ is used to describe the contact angle. Here, the contact angle is defined by the angle between the contact line and the horizontal. The surface tension lies along the contact line about the circumference of the sphere.

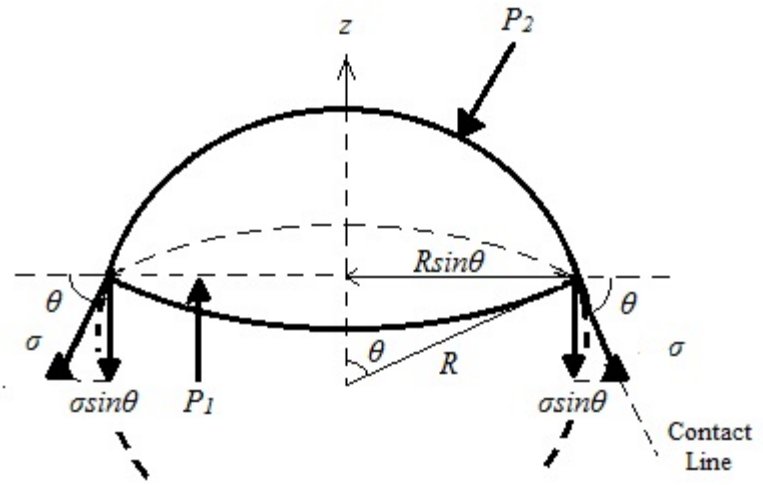

Figure 2.4: Spherical interface.

The area of the spherical interface on which the pressure acts is $A = 2\pi Rh$, where $h = R\text{-}R\cos\theta$. The circumference of the bottom of the interface about which the interfacial surface tension acts is $L = 2\pi R\sin\theta$. Balancing the forces yields the following equation:

$$P_1 A(\theta) = P_2 A(\theta) + (\sigma \sin\theta) L(\theta) \quad (1)$$

In equilibrium, the forces counterbalance each other. Allowing $\theta \rightarrow 90^{o}$, the Laplace equation of capillarity for a spherical interface is obtained.

$$\frac{2\sigma}{R} = P_1 - P_2 \quad (2)$$

2.1.1.2 General Laplace Equation for Arbitrarily Curved Surface

A two-phase fluid system with an arbitrarily curved surface is depicted in Figure 2.4. The pressure difference acting on the area of the interface and the surface tension acting along the perimeter of the interface are shown.

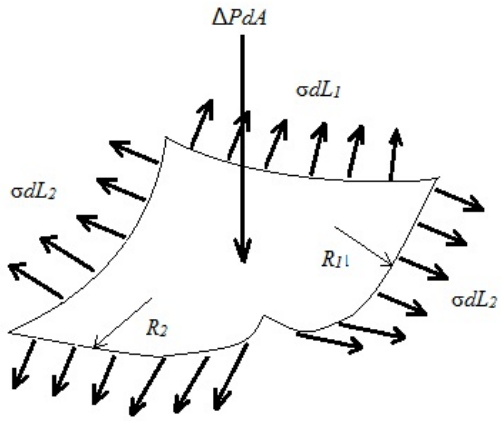

Figure 2.4: Arbitrarily curved interface with radii of curvature, R_1 and R_2.

A force balance normal to the interface as a function of the radii of curvature is given as:

$$\sigma\left(\frac{1}{R_1} + \frac{1}{R_2}\right) = P_1 - P_2 \tag{3}$$

If the two principal radii of curvature are equal, the Laplace Equation reduces to equation (2) for a spherical interface.

2.1.1.3 Laplace Equation for Axisymmetric Fluid Interfaces

In the case where a fluid-fluid interface is interrupted by the presence of a vertical cylinder, the interface forms an axially symmetric meniscus about the cylinder. Two cases showing mensici about two cylinders are described in Figure 2.5.

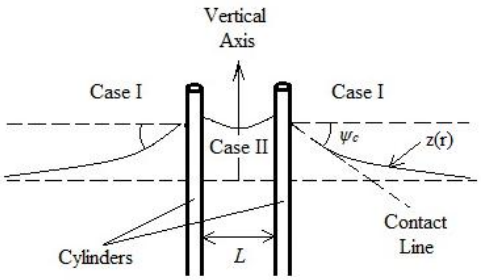

Figure 2.5: Two cases showing menisci formed by the fluid-fluid interface around two vertical cylinders. *L* is the distance between cylinders.

Case I shows a meniscus decaying at infinity on either side of a vertical rod. Ψ_c represents the angle between the horizontal and the contact line and is defined as the slope of the meniscus. The net pressure at the interface is $P = \Delta\rho gz$, where $\Delta\rho$ represents the net density in the two fluids. L is the distance between the two vertical cylinders. Allowing z to equal the boundary between the two fluids and letting r represent the distance from the z-axis, the Laplace equation for a meniscus decaying at infinity can be described by the following form:

$$\frac{z_{rr}}{(1 + z_r^2)^{3/2}} + \frac{z_r}{r(1 + z_r^2)^{1/2}} = \frac{\Delta\rho gz}{\sigma} \tag{4}$$

where $z_r = \frac{dz}{dr}$ and $z_{rr} = \frac{d^2z}{dr^2}$. Gravity cannot be neglected as it is gravity that keeps the surface flat far from the vertical cylinder at the contact line [1].

In Case II, the meniscus forms between two vertical cylinders. The deformation of the interface by the cylinder is analogous to the deformation of a drop of fluid between two parallel plates [1]. The fluid in this case can be decribed as a capillary bridge and takes either a concave or convex shape depending on the wettability of the cylinder. This situation can be formulated by Young's equation.

2.1.2 Young's Equation

Performing a force balance per unit length along a three-phase contact line results in the derivation of Young's equation. The three-phase contact line describes the length along which all three phases on the system meet. In Figure 2.6, the three-phase contact line is perpendicular to the page and is the circumference of the droplet of liquid at the solid surface where all three phases are present. The contact angle within a fluid is defined as the angle between the contact line and the horizontal. In Young's equation, the

contact angle is given in terms of three surface tensions that are present in the system. An equilibrium contact angle is determined by the intermolecular forces that are present at the fluid-fluid interface.

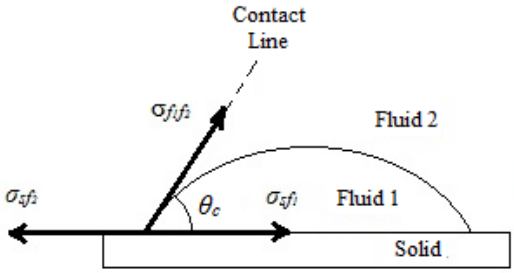

Figure 2.6: Contact line, surface tensions and contact angle revolving about the three-phase contact line.

In the figure above, the three surface tensions, σ_{sf_1}, σ_{sf_2} and $\sigma_{f_1f_2}$ are shown at the Solid-Fluid 1 interface, at the Solid-Fluid 2 interface and at the Fluid 1-Fluid 2 interface respectively. The intermolecular forces at the interface determine the surface tension and the contact angle. Therefore, the contact angle is not dependent on gravitational or other applied external fields but on tension at the contact line [1].

Young's equation derived as depicted in Figure 2.6 is given as:

$$\sigma_{sf_2} = \sigma_{sf_1} + \sigma_{f_1f_2}cos\theta \tag{5}$$

By rotating the diagram in Figure 2.6, the capillary effect as it applies to the thesis experiment can be modeled. The altered diagram in Figure 2.7 is applicable to a chip or micropart sitting atop a mound of liquid. Approximations of surface capillary forces, neglecting other energies, for such a floating body are claculated in section 2.1.3.4 of the chapter.

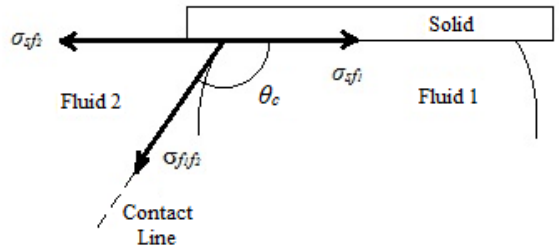

Figure 2:7: Micropart sitting on top of a mound of fluid.

2.1.3 Lateral Capillary Forces

Lateral capillary forces occur when particles are in contact with a fluid boundary and cause deformation in the shape of the interface. A capillary force between two particles on an interface can cause the two particles to either attract or repel each other. As interface deformation increases, capillary attraction or repulsion increases.

There are two types of lateral capillary forces applicable to the present research: capillary flotation forces and capillary immersion forces [1]. Capillary flotation forces occur between floating particles on an interface, as in the example of silicon microparts floating on a liquid-liquid interface. The weight of the microparts is a main contributor to the cause of deformation of the interface. The boundary of a fluid surrounding a body will either rise or depress with the presence of that body on the interface [16]. The weight and the wetting characteristics of a floating particle will determine the shape of the deformation of the interface.

Capillary immersion forces occur between semi-immersed bodies in a fluid. This is represented by vertical rods protruding through a fluid-fluid interface. The deformation of the interface that occurs about a vertical rod takes the shape of a meniscus. The shape of this deformation is dependent upon the wetting properties of the surface of the partially immersed body but is not affected by the body's weight [1].

Two microparts on an interface will attract if both parts cause an upward deformation of the interface or if both parts cause a downward deformation of the interface and will cluster. If two floating parts cause the opposite direction of deformation, they will appear to repel each other [16]. For two floating parts that appear to be attracted to one another, the gravitational potential energy of the two floating parts decreases as the distance between them decreases. Therefore, the lateral capillary flotation force stems from the weight of the particle [16]. More is discussed on this in section 2.1.3.2.

The effect of capillary flotation forces, driven primarily by gravity, and capillary immersion forces, driven primarily by wetting, depend on inter-particle separation. Whether the forces are attractive or repulsive is determined by the slope of the meniscus, ψ, formed around the floating or semi-immersed bodies. Particles with meniscus slopes of the same sign experience attraction and particles with meniscus slopes of opposite signs experience repulsion (Figure 2.8 (a), (b), (d) and (e)). If no meniscus deformation is created on the fluid-fluid interface there is no capillary interaction between particles (Figure 2.8 (c)). This occurs if the weights of the particles are too small to deform the interface [1]. Two particles that deform an interface in the same direction are said to be like particles.

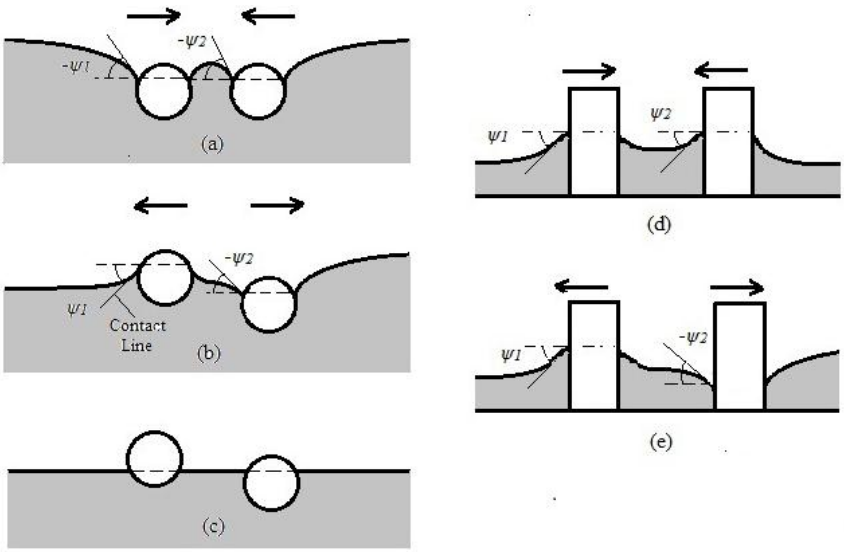

Figure 2.8: The effect of capillary flotation forces driven by gravity and capillary immersion forces driven by wetting. (a) attraction between two similar floating particles, (b) repulsion between a heavy and a light floating particles, (c) no interaction between the particles because no deformation of interface, (d) attraction between two immersed particles, (e) repulsion between two immersed particles

This thesis explores the effects of both lateral capillary flotation and lateral capillary immersion forces taking place simultaneously between horizontal floating microparts and vertical semi-immersed rods. Several previous experimental investigations have been conducted exploring lateral capillary forces between like bodies (pairs of spherical floating particles *or* between pairs of immersed bodies). This thesis aims to analyze the interactions and behavior between both floating tiles *and* vertical, stationary, semi-immersed rods. The goal behind the exploration of both forces is to determine if the cause of the lateral capillary forces can be manipulated to produce a repeatable procedure for ordering micrometer and sub-micrometer parts into 2D arrays. The presence and placement of the semi-immersed vertical rods are the influencing parameters directly related to the mobilization of the microparts.

Lateral capillary flotation and immersion forces exerted on each interacting particle are comprised of a contribution from both an interfacial tension force and a hydrostatic pressure [1]. The lateral capillary force is then defined as:

$$F = F_\sigma + F_P . \quad (6)$$

The force that results from interfacial tension, F_σ, is found by integrating the meniscus interfacial tension, σ, along the three-phase contact line. The hydrostatic pressure, F_P, is derived by integrating along the surface of the particle [1]. For small particles with a radius, $r << (\frac{\Delta\rho g}{\sigma})^{-1/2}$, the contribution of pressure to the lateral capillary force is negligible as $F_P << F_\sigma$ [1]. This assumption is applied to the silicon microparts used in this research. Therefore, the factors contributing to the interactions that are experienced by the floating and immersed bodies from lateral capillary forces are threefold: the wetting energy as it applies to the vertical rod, the gravitational energy as it is experienced by the micropart, and the energy needed to create a meniscus due to deformation of the interface.

2.1.3.1 Lateral Capillary Immersion Force

The lateral capillary immersion force can be depicted with two semi-immersed vertical rods in a fluid-fluid solution. For representation of the lateral capillary force, it is assumed that the interface is axisymmetric about the vertical center of each rod. It is also assumed that the radii of the rods are much smaller than the distance between the two rods.

In Figure 2.9, $\zeta_1(L)$ describes the height of the interfacial meniscus created by the presence of Rod 1. The surface tension at the Rod 2-Fluid 1 interface, at the Rod 2-Fluid

2 interface, and at the Fluid 1-Fluid 2 interface are given as $\sigma_{2,1}$ $\sigma_{2,2}$ and σ, respectively. Ψ_1 defines the meniscus slope between the contact line at Rod 1 and the horizontal.

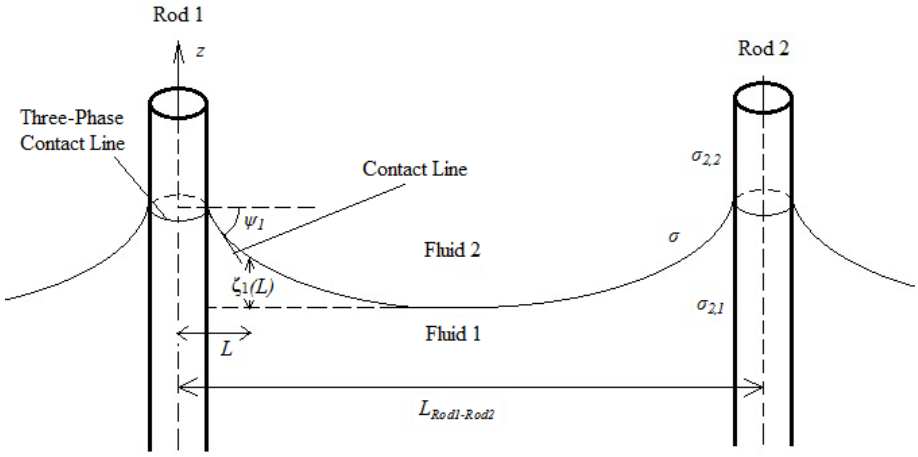

Figure 2.9: Two semi-immersed rods at distance, $L_{Rod1\text{-}Rod2}$, from each other.

In the figure, the level of Fluid 1 around Rod 2 rises with $\zeta_1(L)$. Therefore, the surface area of Rod 2 that is wet by Fluid 1 increases with increase of $\zeta_1(L)$. Likewise, the surface area of Rod 2 that is wet by Fluid 2 decreases with increase of $\zeta_1(L)$ [1].

As previously mentioned, the surface tension force at an interface is described by the surface tension of the interface along the length of the three-phase contact line. For the semi-immersed vertical rods, the three-phase contact line is described by the circumference of the rod. Therefore, the surface tension force at Rod 2 equals the surface tension, σ, times the circumference of the rod, $2\pi r_2$ ($F_\sigma = 2\pi r_2 \sigma$). The surface tension energy is described as the surface tension force along the change in height of the meniscus ($E_\sigma = F_\sigma \Delta\zeta_1(L)$). Therefore, the surface tension energy is defined as the circumference of Rod 2 times the height of the meniscus times the surface tension along the interface. In Reference [1], Kralchevsky and Nagayama describe this energy as the wetting energy along Rod 2 and derive it as:

$$\Delta W_w \approx -2\pi r_2 \zeta_1(L)\left(\sigma_{2,2} - \sigma_{2,1}\right) \tag{7}$$

where r_2 is the radius of Rod 2.

In Equation (7), the surface tension is given as $\sigma_{2,2} - \sigma_{2,1}$. This comes from Young's Equation and could also be expressed as $-\sigma cos\theta_c$ or $-\sigma sin\psi_2$, where θ_c is defined as the contact angle between the contact line at Rod 2 and the vertical surface of Rod 2 and ψ_2 is defined as the slope of the meniscus at Rod 2.

An approximation of the lateral capillary immersion force is formulated by taking the derivative of this wetting energy [1],

$$F \approx \frac{-d\Delta W_w}{dL} \tag{8}$$

where W_w is defined as the wetting energy. Again, this derivation utilizes the approximation that $r_1, r_2 << L$.

2.1.3.2 Lateral Capillary Flotation Force

The cause of attraction or repulsion between two floating bodies can be explained by two contributing factors: deformation of the fluid-fluid interface about one particle and the buoyancy experienced by the second particle [15]. For example, if two like particles create a positive meniscus slope about them and they are laterally near enough to each other, the buoyancy force experienced by the first particle will cause it to move up the inclined interface created by the second particle [15]. The first particle appears to be attracted to the second part as it moves towards it. Likewise, the buoyancy force experienced by the second particle will cause it move up the incline created by the first particle; thus attraction between the two particles is apparent. If, for example, the two

particles create a negative meniscus slope, the first particle experiences a downward gravitational force that is counterbalanced by the present surface tension force [17]. This causes the first particle to move down the depressed interface created by the second particle and they appear to be attracted to one another.

In the case where one floating particle depresses the interface and the second floating particle is wetted by the surrounding fluid, the unlike particles repel each other. Here, the gravitational force experienced by the second particle -encompassing both the buoyancy force and the weight of the particle - is directed upward [17]. Therefore, the second particle floats up the inclined interface around it, moving further away from the first particle. Likewise, it can be said that the first particle moves down the depressed interface around it and moves away from the second particle.

Floating particles seek an equilibrium position at which they would be in the lowest energy state. Like floating particles move toward each other because as the distance between them decreases, the gravitational potential energy experienced by the particles decreases [16, 17]. As the distance between unlike particles decreases, the difference between the meniscus heights of the two particles increases, thus increasing the gravitational potential energy. In the example of the unlike particles described above, the gravitational potential energy, W_g, experienced by the second floating particle can be described as the buoyancy force, F_B, or the gravitational force, F_g, exerted on the particle times the height of the meniscus ($\zeta(L)$) about the first particle [17].

Figure 2.10 shows a particle, representative of a silicon micropart, floating on an interface. The sketch is drawn to show an exaggerated meniscus slope, ψ_1.

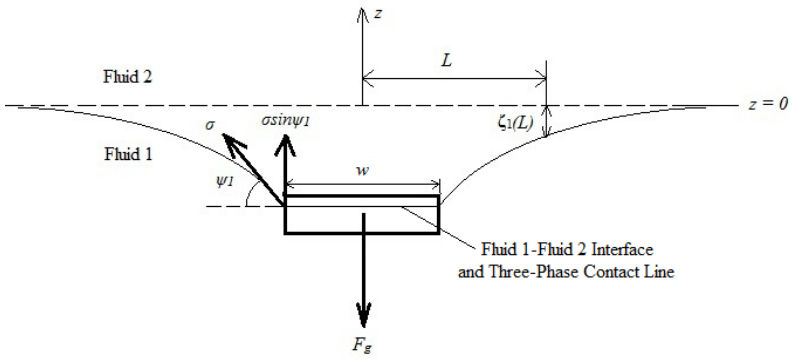

Figure 2.10: Particle on Fluid 1-Fluid 2 interface.

$\zeta_1(L)$ describes the height of the interfacial meniscus about the particle as a function of the distance from the center of the particle. The slope of the meniscus is ψ_1 and the width of the particle is *w*. The length of the three-phase contact line in Figure 2.10 is along the perimeter of the particle and can be described as 4*w*. A second particle, Particle 2, not shown in Figure 2:10, is affected by the meniscus created by Particle 1. Because of the meniscus created by Particle 1, the center of mass of Particle 2 is situated at a distance $\zeta_1(L)$ below the horizontal plane, $z = 0$ [1].

Based on the following assumptions, a function for the lateral capillary flotation force can be approximated. It is assumed that the interface about floating particles is axisymmetric about the vertical axis at the particle's center. The assumption is also made that the particles are small and that the three-phase contact line exists at a constant height. This assumption neglects second order effects that would emerge from a varying height, *(L)*, along the perimeter of the particle and allows for the three-phase contact line to be described as 4*w*. It is also assumed that the angles of inclination or depression of the interface are small. With this assumption, the deformations created by each floating particle are independent of each other. The following derivation also assumes that the

floating particles are small relative to their separation distance (r_1, $r_2 << L$, where r_1 and r_2 are the radii of the particles).

The gravitational force acting on the particle is counterbalanced by the surface tension force which acts along length of the three-phase contact line [15, 17], and can be written as

$$F_g \approx 4w\sigma sin\psi_1 \tag{9}$$

Reference [1] derives the work done by gravity to bring Particle 2 from $z = 0$ down to $-\zeta_1(L)$ as

$$\Delta W_g \approx -F_g\zeta_1(L) \tag{10}$$

As lateral capillary immersion forces can be approximated by taking the derivative of the wetting energy, the lateral capillary flotation force can be approximated by taking the derivative of the gravitational energy, W_g, of a floating particle [1].

$$F \approx -\frac{d\Delta W_g}{dL} \tag{11}$$

The approximations of both the lateral capillary immersion force and the lateral capillary flotation force have the same form and can therefore be compared. Developing an equation explaining the interactive force between a floating particle and an immersed particle is mathematically stable.

2.1.3.3 General Lateral Capillary Force Equation

Kralchevsky and Nagayama derive an expression for the lateral capillary force between a floating and a semi-immersed body separated by a distance, *L*, that encompasses both lateral immersion capillarity and lateral flotation capillarity [1].

$$F \approx -2\pi\sigma \frac{Q_1 Q_2}{L} \tag{12}$$

Q_1 and Q_2 are defined as the capillary charges that Particle 1 and Particle 2 carry, respectively. This equation is analogous to Coulomb's law of electrostatics; hence the term capillary "charge" is derived, where

$$Q_1 = r_1 sin\psi_1 \quad and \quad Q_2 = r_2 sin\psi_2 \,. \tag{13), (14}$$

The sign of the capillary charge is determined by the angle, ψ [1]. Whether the capillary force is attractive or repulsive depends on whether ψ is positive or negative. Like signs for each of the two capillary charges allows for attraction between a floating and a semi-immersed body while opposite signs allow for repulsion.

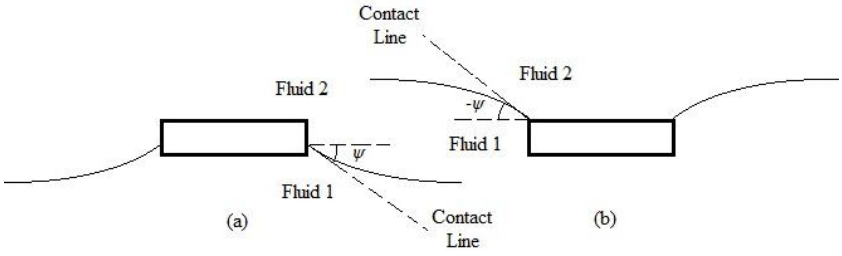

Figure 2:11: Floating particles. (a) positive angle, ψ and (b) negative angle, ψ.

Because the lateral capillary force is a function of ψ, as ψ increases, the lateral capillary force increases. As the distance between a floating and a semi-immersed body decreases, the angle ψ will increase. Therefore, as the spacing between two bodies on an interface decreases, the lateral capillary force experienced by each body will increase.

2.1.3.4 Approximation of Experimental Lateral Capillary Forces

The shape of the interface is determined by the bodies that are deforming the interface. When a floating or semi-immersed body deforms an interface, the contact line along the interface inclines in a positive or negative direction. This inclination is responsible for lateral capillary forces emerging [16]. The interfacial meniscus described as $\zeta(L)$ varies with several factors including the distance, L, between two bodies, the radii of the two bodies, and the wetting properties of the bodies. The change in the shape of the meniscus, $\zeta(L)$, causes change in the center of mass of the particles present and of the fluid. This causes a variation in the gravitational energy described earlier as W_g. [1]. Due to the many factors that contribute to the shape of the interface, it is difficult to derive an exact function to describe the interface. This also makes it difficult to precisely evaluate the lateral forces that are dependent on $\zeta(L)$.

The experiment tested utilizes floating microparts near fixed, semi-immersed, vertical rods. An estimation of lateral capillary forces is calculated for three different scenarios using parameters similar to those in the experiment. First, the lateral capillary immersion force experienced by each of two like semi-immersed rods is estimated. This calculation is not directly related to the experiment but serves as a reference for future computations. Second, the lateral capillary flotation force experienced by each of two like floating microparts is estimated for comparison. Finally, an estimation of the lateral capillary force experienced by both a semi-immersed rod and a floating micropart is conducted to give an idea of the magnitude of the force that is experienced in the thesis experiment.

A rough approximation of the wetting energy experienced along a hydrophobic rod is used to estimate a lateral capillary immersion force experienced by like rods. This is done by approximating the shape of the interface about a hydrophobic rod as $\zeta(L) = ln(x^2 + y^2)$. This function is chosen for simplicity and this shape resembles an interface that is deformed by a hydrophobic rod. The figure below shows a picture taken of the interface during a preliminary investigative trial (Figure 2.12(a)) and a sketch of the function used to represent this interface (Figure 2.12(b)). Though this function is not the exact shape of the interface, it serves as a good approximate representation for the intended calculations.

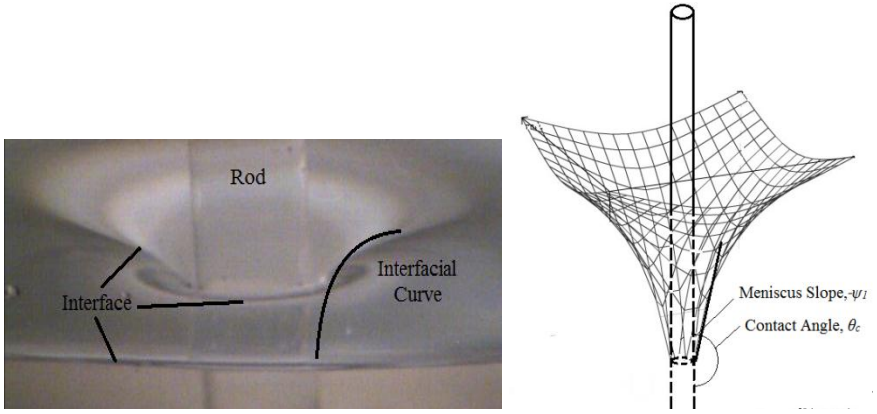

(a) (b)

Figure 2.12: Shape of surface about a hydrophobic rod defined as $\zeta(L) = ln(x^2 + y^2)$. Left image (a) shows picture of interface, right image (b) shows sketch of interface defined by the function.

The wetting energy, W_w, defined by Equation (7) becomes

$$\Delta W_w \approx -2\pi r ln(L^2 + L^2)\,(\sigma cos\theta_c) \tag{15}$$

where x and y are equivalent and equal the distance L and θ_c represents the contact angle between the fluid-fluid interface and the rod. The contact angle is approximated as θ_c = 165º to represent an extremely hydrophobic rod surface. For a vertical rod of radius 0.5

mm, r = 0.0005 m. The experiment uses a water-hexadecane interface. The surface tension of a water-hexadecane interface at room temperature is approximately 52 mN/m [18]. Allowing σ = 52 mN/m, the wetting energy, W_w, becomes

$$\Delta W_w \approx 0.158\, ln(2L^2)\ \text{mN} * \text{m} \tag{16}$$

Differentiating with respect to L gives the lateral capillary immersion force experienced by each rod as

$$F \approx \frac{0.316}{L}\ \text{mN} \tag{17}$$

A rough approximation of the gravitational energy experienced by a silicon micropart is used to estimate a lateral capillary flotation experienced by like microparts. In calculating an approximation of the lateral capillary flotation force, the angle, ψ, will be negative if the micropart on the interface is hydrophobic and positive if the micropart is hydrophilic. Assuming a hydrophobic micropart that creates a small interface deformation, the slope of the meniscus about the micropart is approximated as ψ = 5º. This angle is chosen to implement an extremely small meniscus slope value. It is inferred that the presence of a micropart would form a very small slope of the interface. Using a 500 μm silicon part as is used in the experiment, w = 0.0005 m. The gravitational force experienced by each micropart in the downward direction described by Equation (9) becomes

$$F_g \approx -0.009\ \text{mN} \tag{18}$$

The gravitational energy expressed by Equation (10) becomes

$$\Delta W_g \approx 0.009 \ln(2L^2) \text{ mN} * \text{m} \tag{19}$$

Equation (11) yields an approximation of the lateral capillary flotation force as

$$F \approx \frac{0.018}{L} \text{ mN.} \tag{20}$$

These approximate calculations yield a lateral capillary immersion force experienced by like, 1 mm diameter rods about seventeen times greater than the lateral capillary flotation force experienced by like, 500 μm wide microparts. Based on these rough estimations, it is expected that the presence of the rod will strongly govern the lateral movement of the floating micropart when they are in close proximity.

A rough approximation of the lateral capillary force experienced by both a semi-immersed, hydrophobic rod and a floating, hydrophobic silicon micropart is estimated by using the general lateral capillary force equation. Using the same parameters as were used in the previous calculations, Q_1 defines the capillary charge of the rod and Q_2 defines the capillary charge of the micropart. ψ_1 is approximated as -15° (from Figure 2.12(b)) and r_2 is approximated as half of the width of the micropart. The following capillary charges emerge.

$$Q_1 \approx -0.000129 \quad and \quad Q_2 \approx 0.0000217 \tag{21}$$

Using Equation (12), the lateral capillary forces experienced by both bodies is approximated as

$$F \approx \frac{9.213e^{-}7}{L} \text{ mN} \tag{22}$$

This calculation shows that the lateral capillary forces experienced in the system are extremely small. Graphing the calculated force above versus a range of small separation distances, *L*, yields an exponentially decaying curve of force values (Figure 2.13). These are the estimations of the lateral capillary forces expected to be experienced in the thesis experimental trials. As expected, the approximate calculations show that the lateral capillary force exerted on the bodies is greater for smaller separation distances.

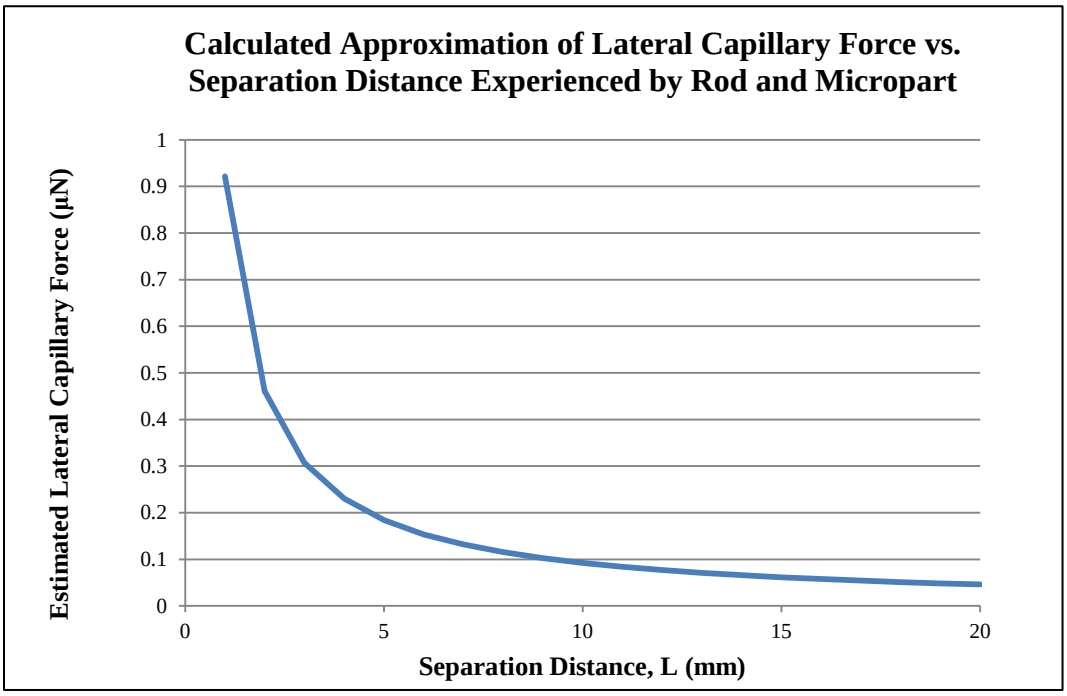

Figure 2.13: Graph of calculated approximate lateral capillary force values.

The lateral attraction or repulsion force is a function of the distance between two bodies. Therefore, it is expected that for two bodies that appear to attract, the lateral force exerted would be positive and would decrease at larger separations. The force between two repelling bodies would be negative and would decrease in absolute magnitude at larger separation distances.

2.2 Previous Work

Several experiments and research studies have been executed in an attempt to gain a further understanding of how surface tension determines the behavior of micro and nano particles. Many of these studies utilized capillary attraction to align microparts by fluidic capillary bridges. Some studies exploring the alignment of microparts on an interface incorporated an electric field.

One recent study aimed to investigate the control of self-assembly of micro and nanoparticles on a fluid-fluid interface by applying an external electric field [7]. In their experiment, Aubry and Singh showed that though similar particles that are on an interface generally cluster, the lattice spacing between particles could be adjusted by applying an electric field and varying the electric field strength. Aubry and Singh placed small glass spheres on separate air-liquid interfaces, each liquid having a different dielectric constant. A vertical electric field was applied normal to the interface.

Aubry and Singh found that for larger sized particles, the buoyancy weight of the particle was much larger than the vertical electrostatic force that the particle experienced. With larger particles, the distance between the particles at equilibrium increased as the electric field intensity increased. For particles of intermediate size, the distance between the particles increased and then decreased with increased electric field intensity. For the submicron sized particles where the buoyancy weight experienced by the particles is negligible, the distance decreased with increased electric field intensity.

Aubry and Singh found that electrostatic forces acting normal to the interface altered the interface deformation initially caused by the particles themselves, which then altered the magnitude of the lateral attractive capillary forces [7]. The electrostatic force

acting parallel to the interface caused repulsion between the particles. It was concluded that by applying an electrical field to the system, the particles polarized and repelled each other via dipole-dipole interactions. Increasing the applied voltage then increased the spacing between the particles in the fluid-fluid interface. The applied voltage must be great enough to create electrostatic forces that overcome the already existing capillary forces.

Research by Sato, et al. established a self-alignment technique for micropart assembly using liquid surface tension [2]. In their experiment, Sato et al. placed a droplet of water on a flat plate and tested the alignment of a micropart to the flat plate caused by the attractive capillary forces in the water droplet using different volumes of water.

Sato et al. placed a droplet of water on the high wettability area of one micropart and then placed a second micropart on top of the first, allowing the droplet to come into contact with the high wettability areas of both microparts [2]. The second micropart was moved by the liquid surface tension of the water droplet so that the high wettability areas of both microparts overlapped. With this, alignment was accomplished.

Sato et al. offset each part's center by 100 μm in relation to each other and placed them at a vertical separation distance of 500 μm. They found that the larger the volume of the water droplet, the more likely the water would overflow into the low wettability area. The smaller the volume of the droplet, the less support there was for the top micropart.

Sato et al. also tested different shaped high wettability areas of the microparts to determine the most accurate alignment technique that lead to no overflow of water and induced a large enough restoring force to inhibit any frictional force. It was concluded that accuracy was compromised if the hydrophobic area of the top micropart that came in

contact with the hydrophilic area of the bottom micropart increased. An increase in alignment accuracy could be attributed to a large restoring force present. Alignment was the most accurate with a hexagonal boundary pattern and the least accurate with a triangular pattern with a high wettability area.

In response to the previous experiment, Tsai et al. developed a technique for self-assembly using surface tension and the solid edge of a protrusion [19]. The experimental set-up was similar to the previous study as there were two microparts that aligned due to the presence of a droplet of water between them. The major difference was that the bottom micropart was represented by a protrusion above the surface of a substrate.

The protrusion replaced the need for surface treatment of the bottom substrate as it confined the water droplet to the protruded area and attempted to prevent overflow. As the contact angle between the drop and the protrusion increased, the likeliness that the drop would spill over decreased as the surface tension in the water increased.

Velez, et al. conducted an experiment where the lateral capillary immersion force between two vertical cylinders at an air-water interface was measured [20]. The lateral force exerted on one cylinder was transferred to a piezo-resistive sensor. The force was converted to an electric signal as a function of the separation distance, L, between the two cylinders.

The capillary force between a hydrophobic cylinder of radius 315 μm and a hydrophilic cylinder of radius 370 μm was tested in pure water. The distribution of lateral force was plotted versus the separation distance between the cylinders. Several distances were tested ranging up to approximately 3 mm. Because the cylinders deformed the interface in opposite directions, the force was negative and repulsive. For the majority of

the data, the distribution curve assumed the shape of a natural logarithmic curve with negative values of force between -5 and 0 μN. For extremely small separation distances, though, where the capillary charge, *q*, times *L* was less than 0.6, the force values did not lie on this curve, but instead took several negative values with no obvious trend.

Velev et al. find that there were three types of forces that were exerted on the vertical cylinder: the hydrostatic pressure within the fluid, the interfacial surface tension, and the lateral force which was dependent on separation distance, *L* [20].

Velev, Denkov, et al. observed the capillary effect between copper beads and a vertical wall on an air-water interface [21]. Solid copper beads of radius 600-700 μm floated a distance from a vertical Teflon plate semi-immersed in the fluid. For plates of different degrees of hydrophobicity, it was found that for larger deformations caused by the plate, a smaller equilibrium separation distance was reached by the copper sphere.

Kralchevsky and Nagayama, in conjunction with the previous experiment, also theoretically calculated an equilibrium distance for the copper sphere [22]. For a fixed contact angle of 89º at the wall, a minimum energy location depicting an equilibrium separation distance was calculated to be where $L/r \approx 0.7$, where *L* was the separation distance and *r* was the radius of the sphere. They found that an equilibrium separation is directly related to the size of the particle and the three-phase contact angle [22].

Kralchevsky and Nagayama reviewed experimental studies involving lateral capillary flotation and immersion forces and gathered the following conclusions [22]:

- Lateral capillary forces appeared when particles at an interface caused perturbations of the interfacial shape [22]. For floating particles, the deformation of the interface was caused by the weight of the particle.

- Lateral forces caused by floating bodies decreased with the sixth power of the particle radius and were not influential for particles with a radius of less than about 10 μm [22].
- Interfacial deformation created by semi-immersed bodies were caused by the wetting properties of the body [22].
- Lateral capillary immersion forces were much more influential and had the potential to be used to manipulate colloidal particles laterally on an interface [22].
- Lateral capillary flotation forces were negligible for spheres with $r < 5–10$ μm, whereas lateral capillary immersion forces could be significant even when $r = 2$ nm [22].

These conclusions agree with the theory explained throughout this chapter.

The studies cited demonstrate methods of implementing surface tension and capillary forces as a method of self-assembly on the micro-scale. Much research has been devoted to this topic in the recent two decades. Further exploration remains necessary to aid in the future development of a self-assembly process that may be used as a method to manufacture and assemble microparts in high production.

Chapter 3:

Geometric Model of Fluid-Fluid Interface

The modeling software, Surface Evolver, was used to create a simulated liquid-liquid interface to represent the geometry of the surface of the experimental set-up. The model serves as a preliminary step that could lead to future calculations of energies and forces present in the system. The geometrically simulated interface establishes the groundwork for future analysis and computations not conducted in this thesis.

The purpose of the experiment, later described in detail in Chapter 4, is to test the effect of a deformed fluid-fluid interfacial shape on a micropart floating on the interface. The interface deformation is caused by the presence of vertical, 1 mm diameter rods. The rods represent semi-immersed bodies that penetrate the interface. In practice, the vertical rods that are hydrophilic cause the interface to form a concave meniscus about the rod. Hydrophobic rods create a convex meniscus. In the experiment, either hydrophilic or hydrophobic rods are equally spaced in an array and a 500 μm x 500 μm x 10 μm silicon tile is placed between them. The behavior of the silicon micropart is observed as it is influenced by the different surface geometries.

The modeling software, Surface Evolver, integrates fluid surfaces and constraints to calculate the energy of the system. The model constructed here can include both interfacial energies and gravitational energy. The equilibrium configuration is found by solving for that surface which minimizes the system energy subject to the applied

constraints [23]. Forces are calculated from the derivative of the energy with respect to displacement of the micropart along the interface [23].

The Surface Evolver model of the fluid-fluid interface incorporates a floating silicon micropart of the above mentioned dimensions by omitting a 500 μm x 500 μm square from the surface. The 1 mm diameter rods are represented by the absence of four circles, spaced 2 mm apart, on the surface. Figure 3.1 below shows a top view of the modeled surface.

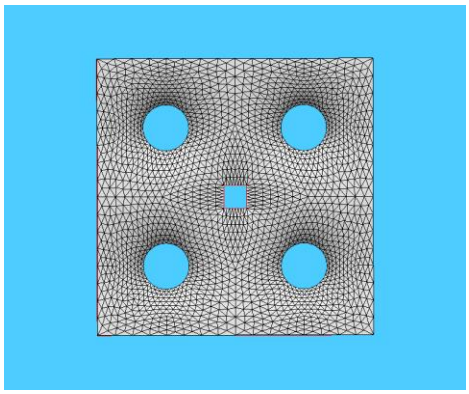

Figure 3.1: View of modeled surface from above. Surface includes four equally spaced holes with a diameter of 1 mm to represent the presence of vertical rods. The square at the center represents the presence of a micropart.

The parameters that are defined in the model, including the dimensions and locations of the rods and the dimensions of the micropart and fluid surface, are written as parameters in the model. These parameters may be altered with the start of a new run of a simulation. The location of the micropart may be altered during an existing run of the Surface Evolver program by use of a lateral shift command, as shown in Figure 3.2.

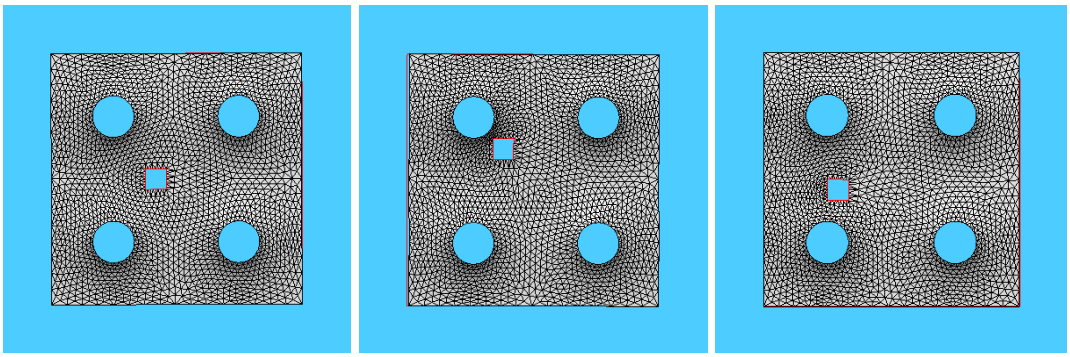

Figure 3.2: Manipulation of location of micropart on modeled surface.

The model is constructed so that a capillary height, also referred to as the height of the meniscus, may be defined along the surface of the rods. This parameter, too, may be altered when starting a new run of the simulation. For a defined capillary height that is greater than the height of the surface, a concave meniscus is created about the rods. A convex meniscus about the rods is created for a defined capillary height that is less than the height of the surface. Adjustment of the capillary height at the surface of the rods allows for creation of surface geometries that implement representations of both hydrophilic and hydrophobic rods. Figure 3.3 below shows views of a surface with concave menisci formed about the rods.

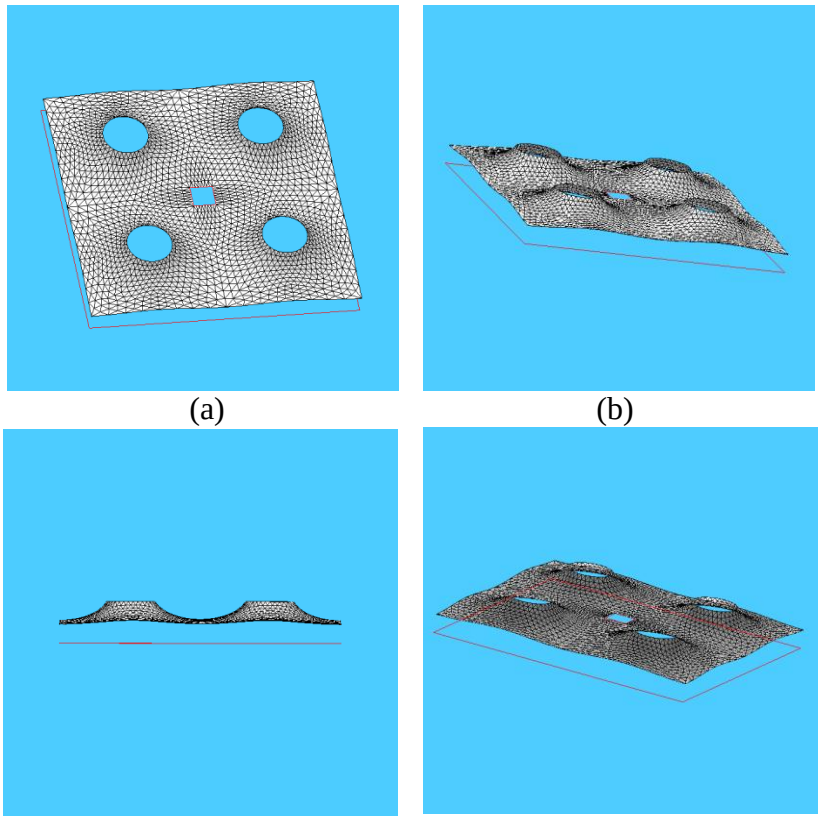

(a) (b)

(c) (d)

Figure 3.3: Modeled surface in which capillary height is defined as higher than the middle of the surface. Views of surface are from (a) above, (b) above, angled, (c) side and (d) underneath.

Figure 3.4 shows views of a surface where convex menisci are formed about the rods.

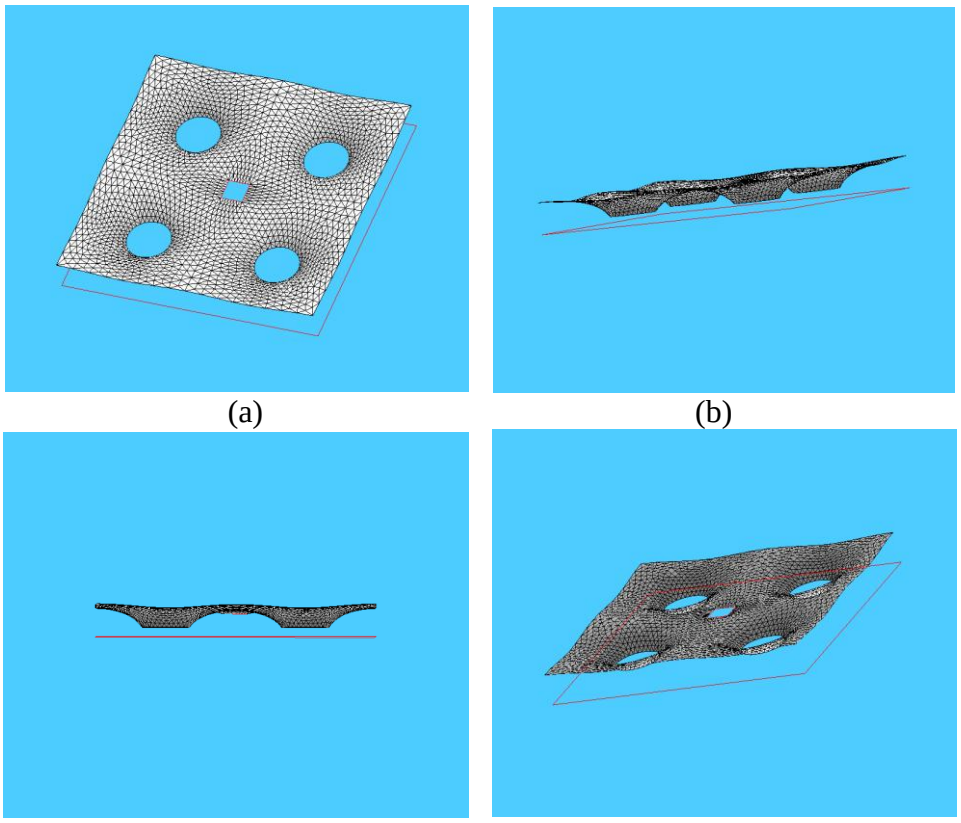

(a) (b)

(c) (d)

Figure 3.4: Modeled surface in which capillary height is defined as lower than the middle of the surface. Views of surface are from (a) above, (b) above, angled, (c) side and (d) underneath.

Surfaces for two different rod spacing arrangements were created for modeling of varying spacing parameters, keeping all other dimensional parameters constant. The first configuration is used in the previous figures of this chapter. A second surface applies twice the distance between rods; 4 mm. Both surfaces are shown in the figure below for comparison.

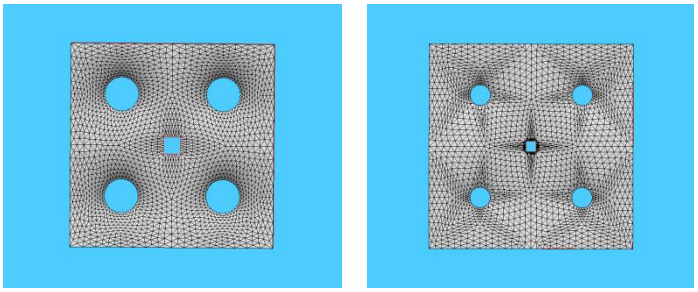

(a) (b)

Figure 3.5: Modeled surfaces showing two rod spacings. (a) 2 mm rod spacing and (b) 4 mm rod spacing.

Simulations involving both surface configurations may be useful in future calculations.

Constraints are implemented into the model along the circumference of the rods and the perimeter of the micropart. The energy of the wetted surface of the rods is calculated from an integration of the wetted area around the rod constraint. The surface tension is defined for a liquid-liquid interface and integrated across the area. The energy of the surface about the micropart is also defined by the surface tension integrated along the edges of the micropart constraint. The potential energy of the micropart as a function of its mass also contributes to the surface energy surrounding the rod. The surfaces of the rods and micropart are represented by the edge integrals to improve stability and convergence of the Surface Evolver model [24].

The foreseen future application of the geometric model of the surface is an accessory in calculation of the lateral capillary forces that are experienced by the micropart for different surface configurations as a function of micropart location. Surface energy calculations may also be useful in developing future work.

Chapter 4:

Experimental Design

This chapter outlines an explanation for the experimental methods and parameters. Fabrication and treatment of equipment is described. The experimental variables are explained and procedures for carrying out the prescribed trials are given.

4.1 Basic Experimental Design Description

The research experiment is designed to achieve an event where the effects of lateral capillary forces can be observed. Therefore, a fluid-fluid interface must be present along which both capillary flotation forces and capillary immersion forces can occur.

The experimental set-up must utilize bodies whose interaction results in a lateral capillary force that may be classified as both a capillary flotation force and/or a capillary immersion force. To satisfy this requirement, there must be two types of bodies between which the force emerges. One body must be floating on the fluid-fluid interface. The second body must be semi-immersed so that it is supported by a solid substrate that lies below the fluid-fluid interface, and the top of the body must extend through the fluid-fluid interface and protrude above it.

A bath of deionized water in an open container provides an interface at the top surface of the liquid and the ambient air. In this experiment, hexadecane, immiscible with water, is added to create a liquid-liquid interface. A description of the liquid-liquid

interface as it meets the requirements of experimental goals is discussed in section 4.3.3 of this chapter. Figure 4.1 depicts a side view of vertical rods immersed in a hexadecane-water bath and a micropart floating at the interface.

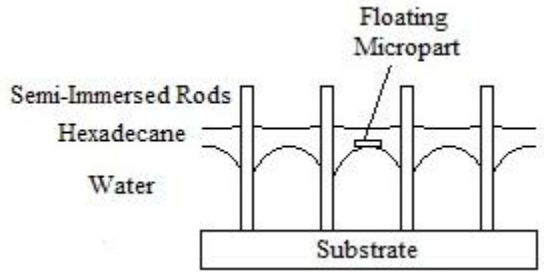

Figure 4.1: Side view of semi-immersed rods and floating micropart on a hexadecane-water interface.

A thin vertical rod placed in the bottom of the enclosed container and tall enough to protrude through the liquid-liquid interface serves as a body that can be classified as semi-immersed. Incorporating an aluminum plate (130 mm x 106 mm x 6.5 mm) with a rectangular array of 1.0414 mm diameter holes spaced 3.1 mm apart provides a weighted fixture. This fixture sits in the base of the open container in the bottom of the liquid bath and supports the vertical, cylindrical rods.

A thin, square tile whose characteristics are representative of a micropart used in photovoltaic solar cells serves as a floating body. A detailed description of the microparts is given in section 4.3.2 of this chapter. When the micropart is placed on the liquid-liquid interface in the presence of vertical semi-immersed rods, lateral capillary forces emerge between the micropart and the rods. The magnitude of these forces is relative to the proximity of the micropart to the rods.

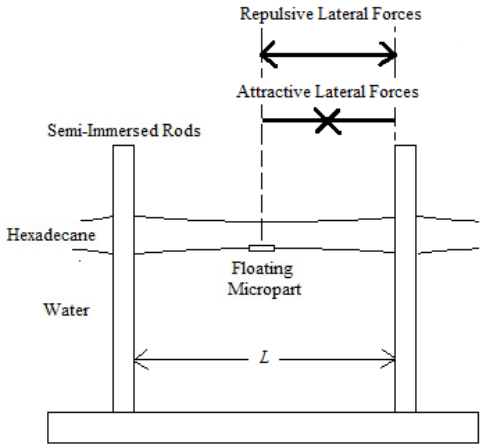

Figure 4.2: Side view of repulsive and attractive lateral capillary forces.

As previously discussed, capillary flotation forces occur between floating bodies and capillary immersion forces occur between semi-immersed bodies. This experimental set-up is designed to include both floating and semi-immersed bodies so that the lateral capillary forces that result between them can be categorized as both capillary flotation forces and capillary immersion forces.

4.2 Measured Experimental Quantities

The physical experiment documents empirical observations to show the effect of lateral capillary force on separation distance. Because force cannot be directly measured in the experimental set-up, the behavior of the micropart is instead observed, and this will determine the direction of the force.

As the micropart is placed on the liquid-liquid interface during the experimental trials, it migrates in a direction that is hypothesized to be determined by the lateral capillary force that results from the presence of the vertical rods. This movement of the micropart along the interface occurs immediately upon release onto the interface and continues until the micropart reaches a location where it is in equilibrium. The micropart

moves rapidly at first and then its velocity decreases and may become zero. The time that the micropart takes to reach a constant distance from the rod after it is placed on the interface is referred to as the "equilibrium time." The distance from the center of the micropart to the closest rod when it reaches the equilibrium time is referred to as the "equilibrium distance."

The experiment documents the equilibrium distance that the micropart reaches. It is inferred that the shorter the equilibrium time, the stronger the lateral capillary force acting on the micropart. The equilibrium distance that the micropart reaches in relation to its initial launch onto the interface determines if the lateral capillary force between the micropart and closest rod is positive or negative, meaning attractive or repulsive.

By documenting equilibrium position and monitoring the direction of travel by the micropart, a dimensionless description of the lateral capillary force can be constructed.

A total of sixteen equally spaced rods are used in each trial. The experiment focuses on what occurs between the four central rods. The surrounding twelve rods serve to create symmetry in the experimental set-up. A single micropart is released onto the liquid-liquid interface between the four, centrally located adjacent rods. One of the four rods acts as the 'closest rod' and is defined by the location at which the micropart is placed on the interface. The micropart is placed on a diagonal distance approximately one quarter of the distance to the closest rod. The rod that is determined to be the closest rod maintains that distinction through the remainder of the trial. Figure 4.3 depicts a top view of the rods and the placement of the micropart.

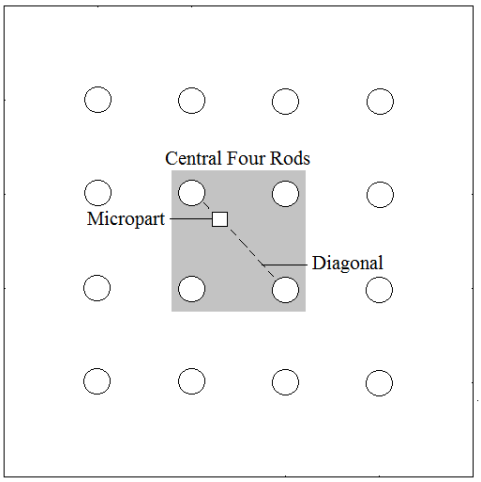

Figure 4.3: Placement of micropart one quarter of the distance along the diagonal. Shaded grey area highlights the four central rods.

The placement location has been chosen as a position where the forces contributed by the closest rod will dominate the motion of the micropart. Also, a quarter of the distance along the diagonal allows for both repulsive and attractive movement of the micropart. The distance, *L*, from the center of the micropart to the outside diameter of its closest rod, is documented throughout each sixty second trial from the initial release of the micropart.

4.3 Experimental Components

The vertical rods and the microparts used in the experiment are described and the liquid-liquid interface is explained.

4.3.1 Rods

The rods used in the experiment are quartz glass, chemical formula SiO_2. The rods have an outside diameter of 1 mm and are approximately 2.5 cm in height. The vertical rods are long enough to stand upright from the bottom of the open container and

protrude through the liquid-liquid interface. This arrangement allows each rod to be classified as a semi-immersed body that creates lateral capillary immersion forces.

The influence of lateral capillary forces is observed for different interface distributions. When a vertical rod interrupts the liquid-liquid interface, the interface is deformed at the rod. The quartz glass rods are naturally hydrophilic. Therefore the interface deforms upward along the surface of the rod to form a concave meniscus about the rod (Figure 4.4). The deformed shape of the interface influences the magnitude and direction of the lateral capillary force experienced.

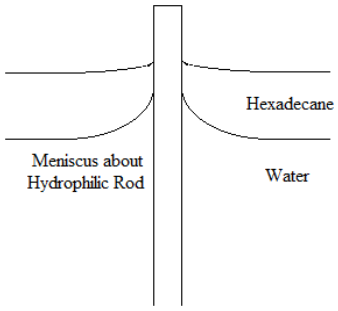

Figure 4.4: Concave meniscus formed about the rod.

To observe the effects of the capillary forces between the microparts and the rods it is also necessary to test a convex liquid surface. Treating the quartz glass vertical rods to become hydrophobic reverses the curvature of the liquid-liquid interface (Figure 4.5).

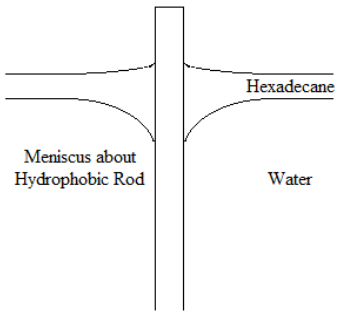

Figure 4.5: Convex meniscus formed about the rod.

An ideal characteristic of the quartz glass is that it can easily be treated at a minimal cost to become hydrophobic. This allows for testing of both concave and convex surface deformations. A description of the treatment of the rods to render them hydrophobic is given in section 4.5 of this chapter.

4.3.2 Microparts

The microparts tested in the research are crystalline silicon. The silicon microparts float at the liquid-liquid interface when released into the system. The microparts therefore represent bodies that create lateral capillary flotation forces. When placed on the interface, the microparts, treated to be hydrophobic, slightly deform the interface in a negative direction, making a slight negative meniscus slope, ψ_M, between the interface and the horizontal (Figure 4.6). A description of their treatment is given in section 4.4 of this chapter.

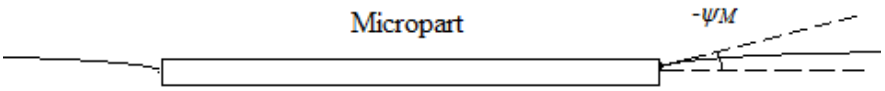

Figure 4.6: Hydrophobic micropart slightly deforming the interface, causing a slight negative meniscus slope.

Crystalline silicon is essential in developing technology for electronic devices and, more relevantly, solar cells. A significant application of the experimental data collected is to determine the feasibility of a large scale fabrication method for manufacture of photovoltaic cells. Silicon is the appropriate material choice for the microparts as photovoltaic cells are constructed of crystalline silicon [14]. The silicon microparts are representative of microparts that would be used to assemble solar cells on a broad size scale. An array of silicon microparts could form a solar panel of a desired

size. Using capillary forces to manipulate the movement of silicon microparts into an array would be an innovative method of solar cell fabrication yet to be developed.

The silicon micro-tiles used in this work are 500 μm long, 500 μm wide and 10 μm thick. Additional trials utilize 1 mm x 1 mm x 10 μm parts and 250 μm x 250 μm x 10 μm parts. The dimensions are representative of microparts that would be used in the assembly of photovoltaic solar cells and are also ideal for ease of fabrication on site. The fabrication process of the silicon microparts is described in section 4.4 of this chapter.

4.3.3 Hexadecane-Deionized Water Interface

The purpose of the experimental research is to observe the movement of the microparts that occurs due to the curved surface topography that is created by the vertical rods. It is hypothesized that more movement will take place in a setting where the contact angle of the capillaries is large.

At liquid-liquid interfaces, the difference in densities of the two fluids is less than at liquid-gas and liquid-solid interfaces [7]. By minimizing such differences, the gravitational resistance that the lower, denser liquid experiences at the interface is reduced. This allows for more pronounced capillary height effects at the surface of the denser liquid.

Two immiscible liquids, such as oil and water, form a stable liquid-liquid interface. The oil has the desired effect of increasing the curvature of the surface of the water as described above. The oil also increases the surface curvature of the water in the presence of vertical rods that are rendered hydrophobic. The surface energy effects that occur by having the oil ambient to the water surface cause the contact angle between the hydrophobic rod and water to increase. The curved surface created by the hydrophobic

rods is also encased on the oil-water interface. In the presence of hydrophilic rods, the oil causes the contact angle to decrease. This is a desirable effect as it is hypothesized that a more dramatically curved surface will manipulate the microparts more strongly. The oil, therefore, allows for more measurable results.

Hexadecane is chosen as the ambient oil as it is chemically homogeneous and is easily obtainable at a relatively inexpensive cost. Deionized water is used to minimize the incidental effects impurities on the surface energy.

4.4 Fabrication of Silicon Microparts

The silicon micro-tiles are fabricated via standard photolithography and etching techniques. A thin film of chromium and a thin film of gold are deposited by e-beam deposition on a crystalline silicon on insulator (SOI) wafer. The SOI wafer consists of a 10 μm thick silicon (100) device layer and a 1 μm thick silicon dioxide layer. The e-beam induced deposition of a 20 nm layer of chromium occurs at a rate of 5 Å/s and a 200 nm layer of gold is deposited at 2 Å/s over the chromium.

A 1.2 μm thick Shipley 1813 photoresist is used during photolithography. The photoresist is exposed to 20 mW of ultraviolet light for 5 seconds. Transene etchant is applied to etch the gold layer at 25ºC and the chromium at 40ºC. The 10 μm thick silicon device layer is etched by deep reactive-ion etching (DRIE) via an Alcatel DRIE tool. Finally, the microparts are released from the surface of the SOI wafer by exposing the wafer to hydrofluoric acid vapor of 50% concentration in water. Silicon is naturally hydrophobic, but exposing the microparts to hydrofluoric acid ensures that any oxide layer that may cause the parts to be hydrophilic is not present. After fabrication, the microparts are stored in isopropyl alcohol to minimize oxidation of the silicon.

4.5 Treatment of Quartz Rods

To get an exaggerated contact angle between the rods and the surface of the deionized water, Rain-X® is directly applied to the quartz rods to render them hydrophobic. Rain X® is a silicone polymer whose primary active ingredient is hydroxyl-terminated polydimethylsiloxane that binds to the hydroxyl group of a glass surface [25]. Pure Rain-X® produces a hydrophobic surface on the rod that is a dramatic contrast to the untreated, hydrophilic surface. With a large contact angle present, a distinct comparison of results may be made in the direction of motion of the microparts between untreated rod trials and treated rod trials.

The rods are completely submerged in a bath of Rain-X® for one minute and then removed. The rods are individually gently buffed with Kimberly-Clarke® Kimwipes until a hazy film forms on the rods. Separate Kimwipes are then used to gently buff away the thin layer of haze.

4.6 Experimental Variables

The variables of the experimental research were developed from pre-trial observations made during testing microparts on a hexadecane-deionized water interface in the presence of untreated, hydrophilic quartz rods.

Five spacing distances between the rods are tested. The distances tested (2.1 mm, 5.3mm, 8.5 mm, 11.7 mm and 14.9 mm between rod outer diameters) are based on the placement of the pre-drilled holes in the aluminum plate. Further spacing than what is defined in the five trials is extraneous and leads to no significant relationship between the rods' influence on the mobilization of the microparts.

Testing for the two cases of using untreated rods that are hydrophilic and treated rods that are hydrophobic allow for comparison between the two sets of trials. The shape of the deformation of the interface is either a concave or convex meniscus about the rod and determines whether the floating and semi-immersed bodies attract or repel.

As mentioned, the microparts form a slight negative angle, ψ, with the interface. It is hypothesized that in the case of hydrophilic rods where the meniscus slope formed by the rods, ψ_R, is positive, the microparts will repel from the rods and gravitate towards the middle of the open area of the interface. For hydrophobic rods where the meniscus slope, ψ_R, is negative, it is expected that the microparts will be attracted towards the rods. Like directions of the angles ψ_R and ψ_M, caused by the rods and the microparts respectively, will cause attraction while different signs of the angles will cause the two bodies to repel from each other. This hypothesis is demonstrated in Figure 4.7 below.

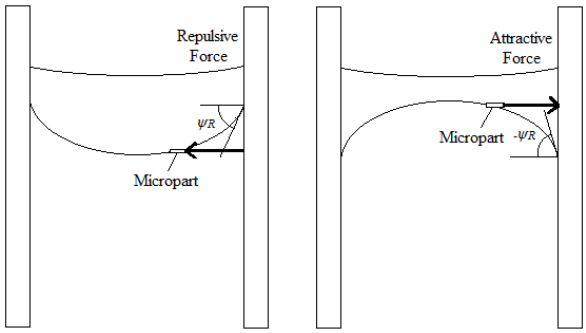

Figure 4.7: Hypothesized direction of lateral force exerted on micropart. Direction in the presence of (a) hydrophilic rod and (b) hydrophobic rod.

4.7 Experimental Set-Up and Procedure

Video is taken of the array of sixteen vertical rods for documentation. One micropart is used in each trial and placed between the rods as shown in Figure 4.3 above.

Data of the position of the micropart located in the center of the rods is recorded as it represents a part located in any position within an array of any size.

Before each trial, the quartz rods are cleaned in a Blazer Digital Ultrasonic Cleaner 4800 in an acetone bath, a methanol bath and then a deionized water bath for 180 seconds each, at 42,000 Hz. Once dry, the clean, untreated quartz rods are used for trials where hydrophilic rods are needed. They are then inserted into holes of the aluminum plate so they stand vertically. For the trials using hydrophobic rods, the rods are treated with RainX® before being inserted into the aluminum plate. The aluminum plate is 130 mm x 106 mm x 6.5 mm with Ø1.0414 mm holes drilled through it. The holes are spaced 3.1 mm apart, center to center. The rods are placed at a desired spacing according to the trial, leaving 2.1 mm, 5.3 mm etc. between rods, outer diameter to outer diameter.

The aluminum plate is placed in the bottom center of a square Pyrex bowl. The Pyrex square bowl is filled with 400 mL of DI water to create a 1 cm tall bath above the aluminum plate. A four walled glass box made from four 2 in x 3 in x 1 mm glass microscope slides is placed on top of the aluminum plate, around the array of rods, to act as a boundary for the hexadecane layer. With a dropper, 20 mL of n-Hexadecane, 99%, purchased from Alfa Aesar, is placed on the surface of the DI water inside the boundaries of the glass box to create an approximately 3 mm thick layer of hexadecane. Figure 4.8 shows the experimental set-up.

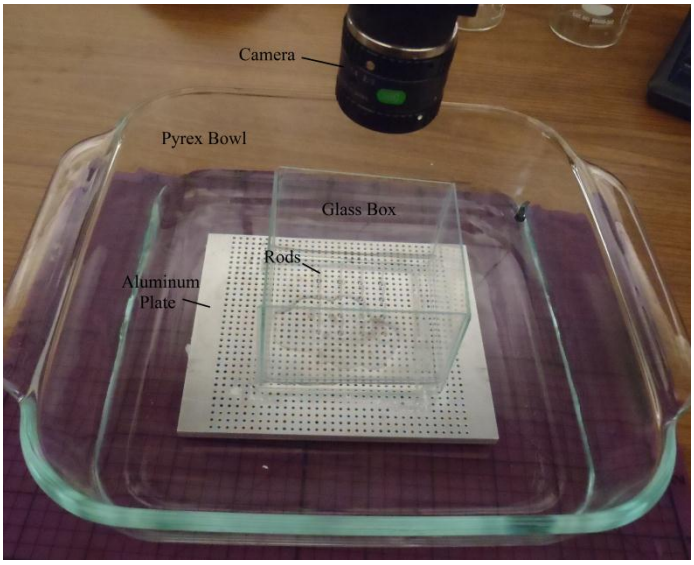

Figure 4.8: Picture of experimental set-up.

Separately, a syringe is used to pick up the individual micropart (Figure 4.9(a)). No suction or pressure is created by the syringe, nor do the microparts enter its tip. A syringe is used because a micropart can lay flat against the tip of the syringe. The flat placement on the end of the syringe also allows for a relatively consistent deposition of the micropart onto the interface. Alternatively, the microparts are too brittle to be manipulated by a needle or tweezers without breaking. While keeping the syringe as vertical as possible, the syringe is gently lowered so that its tip is placed through the surface of the hexadecane and through the water-hexadecane interface so that the tip barely penetrates the interface (Figure 4.9(b)). This releases the micropart from the tip of the syringe and into the top of the volume of DI water just below the interface. The micropart immediately floats to the water-hexadecane interface and remains trapped at the interface. While continuing to keep the syringe vertical, it is gently raised to remove the tip from the fluids (Figure 4.9(c)).

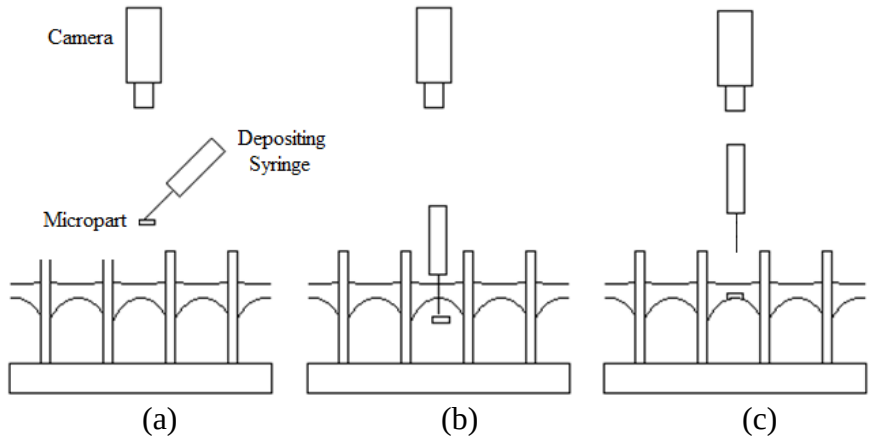

Figure 4.9: Deposition process of the micropart onto the interface. (a) before release, (b) just after poking syringe tip through interface and (c) after deposition.

Digital video records each trial using an Edmund Optics® 2.0 CMOS USB Camera with a 12 mm lens and is documented via uEye capturing device software. From the digital video, thirty-two still pictures are extracted over the sixty second trial, beginning with the initial release of the micropart onto the interface. Twenty-one pictures are extracted from the first ten seconds; one every half second, then one every second for the next five seconds. Thereafter, a picture is extracted at 20, 25, 30, 40 50 and 60 seconds. Each of the extracted images is viewed in uEye where the location of the micropart and center of the closest rod are measured with the software measuring tool. The separation distance for each image is calculated and recorded. The majority of the movement of the micropart takes place in the first few seconds of the trial and the described intervals of sequencing captures this.

Some sets of trials utilize hydrophilic quartz rods creating a concave interface, others use hydrophobic rods creating a convex interface. With respect to each set, a separation distance versus time graph documents the movement of the micropart for each spacing arrangement. The separation distance, *L*, is defined as the distance between the midpoint and the micropart to the outer diameter of the closest rod.

As described in Figure 4.7 above, it is hypothesized that for a positive meniscus slope, ψ_R, the micropart will repel away from the vertical rod and that for a negative meniscus slope, ψ_R, the micropart will travel to the vertical rod.

Chapter 5:

Experimental Results and Discussion

The empirical data for all of the trials carried out in the experiment are presented and analyzed. The results show the effects of surface tension created by the presence of vertical rods on the movement of the silicon microparts by displaying the separation distance of the micropart throughout each trial.

5.1 Hydrophilic vs. Hydrophobic Rods: Influence on Hydrophobic Micropart

The initial set of trials aims to observe how different spacing arrangements of both hydrophilic and hydrophobic rods affect the movement of a micropart. Subsets of trials contain different lengths of spacing between rods. Each subset contains five trials. In each trial a new micropart is used. A list of the trials conducted in the first set is shown in Table 5.1 below.

Table 5.1: List of first set of trials. hydrophilic and hydrophobic rods for different spacing arrangements using hydrophobic microparts

Hydrophobic Microparts	
Hydrophilic Rods	Hydrophobic Rods
2.1 mm Rod Spacing/3.38 mm Diag. (5 Trials)	2.1 mm Rod Spacing/3.38 mm Diag. (5 Trials)
5.3 mm Rod Spacing/7.91 mm Diag. (5 Trials)	5.3 mm Rod Spacing/7.91 mm Diag. (5 Trials)
8.5 mm Rod Spacing/12.44 mm Diag. (5 Trials)	8.5 mm Rod Spacing/12.44 mm Diag. (5 Trials)
11.7 mm Rod Spacing/16.96 mm Diag. (5 Trials)	11.7 mm Rod Spacing/16.96 mm Diag. (5 Trials)
14.9 mm Rod Spacing/21.49 mm Diag. (5 Trials)	14.9 mm Rod Spacing/21.49 mm Diag. (5 Trials)

The rod spacing shown is defined by the distance between adjacent rods from outer diameter to outer diameter. The distance between diagonally spaced rods as they correspond with the adjacent rod spacing is also given. Figure 5.1 depicts the closest spacing arrangement.

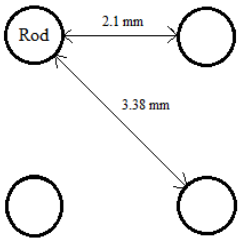

Figure 5.1: Top view of 2.1 mm rod spacing between adjacent rods and 3.38 mm diagonal spacing between diagonal rods.

In the first set of trials, hydrophilic rods cause the hexadecane-water interface to rise along the surface of the rods, deforming the surrounding interface. Further away from the rods, where there is no semi-immersed body present to interrupt the surface, the interface is assumed to be flat and is lower than the height of the interface touching the rods, as shown in Figure 5.2.

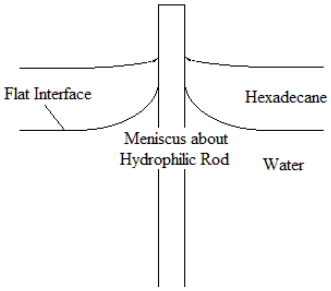

Figure 5.2: Shape of interface about hydrophilic rod.

For the largest spacing distance tested, 14.9 mm between adjacent rods, this flat area of the interface is the widest. As the spacing decreases between rods, this flat area decreases in size. For the shortest rod spacing, 2.1 mm between rods, a flat area of the

interface is nonexistent between adjacent rods as the meniscus surrounding each rod intersects the meniscus of the adjacent rod, as shown in Figure 5.2.

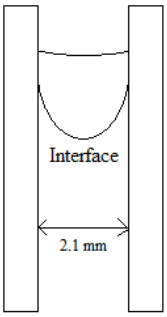

Figure 5.3: Two menisci intersecting between closely spaced hydrophilic rods.

Also in the first set of trials, hydrophobic rods that cause a convex hexadecane-water interface are tested using the different spacing arrangements. The interface that lies away from the rods is assumed to be flat and is raised higher than the height of the interface touching the rods (Figure 5.4).

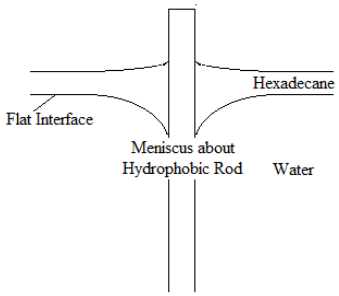

Figure 5.4: Shape of interface about hydrophobic rod.

For the shortest rod spacing, the interface takes a complete convex shape and no flat portion is present between adjacent or diagonal rods (Figure 5.5, Figure 5.6).

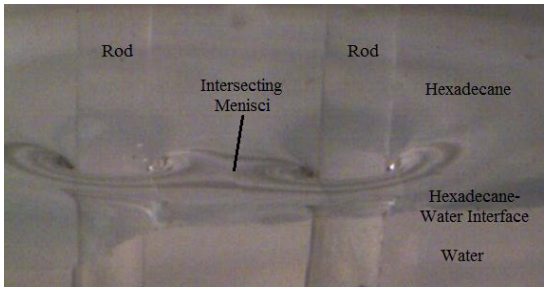

Figure 5.5: Picture of two menisci intersecting between hydrophobic rods spaced 2.1mm apart.

Figure 5.6: Picture of two menisci intersecting between hydrophobic rods spaced 3.38 mm apart.

In every trial, the micropart is deposited approximately one quarter of the length of the distance from the closest rod to its diagonal counterpart.

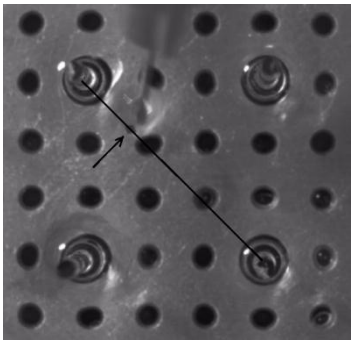

Figure 5.7: Diagram showing placement location of micropart on diagonal approximately one quarter of the length of the diagonal spacing.

The movement of the micropart along the interface is shown in the graphs displayed below. Each graph presents data for a single rod arrangement. The graphs display the distance of the micropart from its initial release onto the interface through the

one minute trials. The distance, *L*, is defined as the separation distance between the midpoint of the micropart and the outer diameter of its closest rod. The method for measuring this distance is described in Chapter 4. Each line on the graph represents a single trial, each with a new micropart. The dotted lines depict trials where hydrophilic rods are used and the solid lines show trials where hydrophobic rods are used. The different colors of the lines do not denote any particular parameter but are used for ease of deciphering separate lines. The separation distance of the micropart as it is influenced by both the hydrophilic and hydrophobic rods is shown on each graph for comparison, starting with Figure 5.8 below.

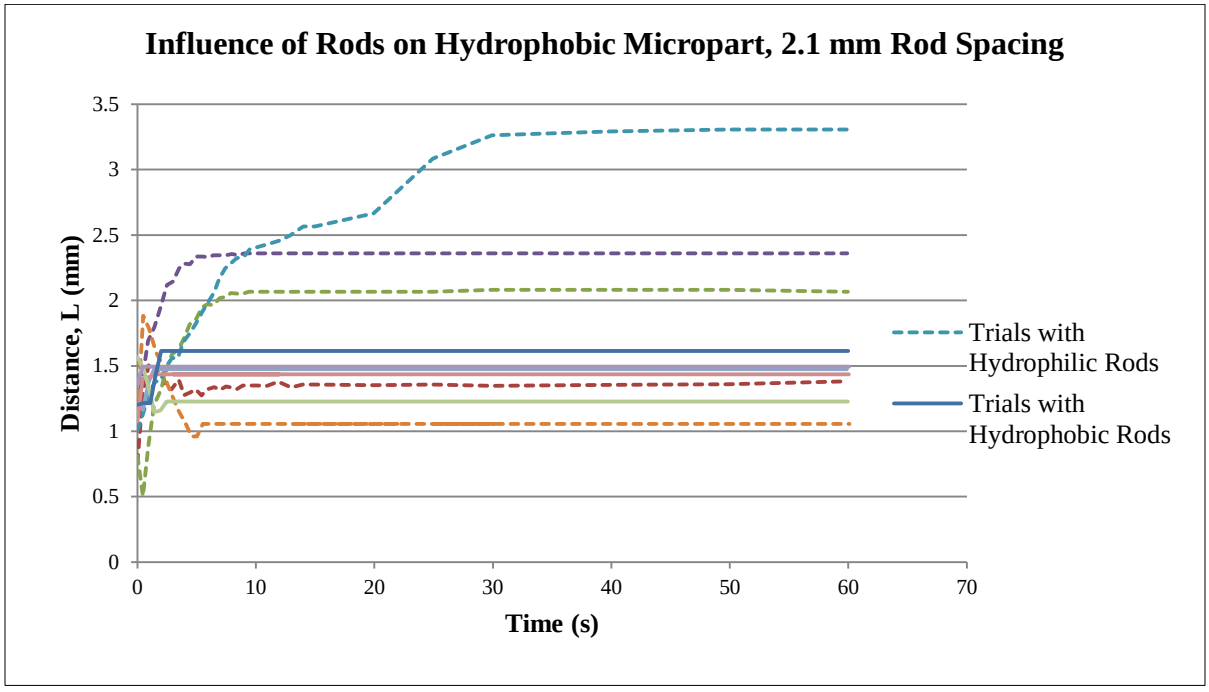

Figure 5.8: Graph of 2.1 mm rod spacing. Hydrophobic part with both hydrophilic and hydrophobic rods.

In the trials using the hydrophilic rods, the microparts do not show a preferred direction of travel either toward or away from the rod after initial placement. They do, though, find an equilibrium distance and cease travel before the end of the sixty second

trial. In some cases, during movement, a micropart slightly rotates about its z-axis. In four of the five trials with hydrophilic rods, the micropart reorients itself, spinning slightly until an edge of the micropart faces the closest rod (Figure 5.9). This edge becomes almost parallel with the tangent to the location on the rod diameter that the micropart is traveling toward (Figure 5.10). The spinning ceases before the equilibrium distance is reached.

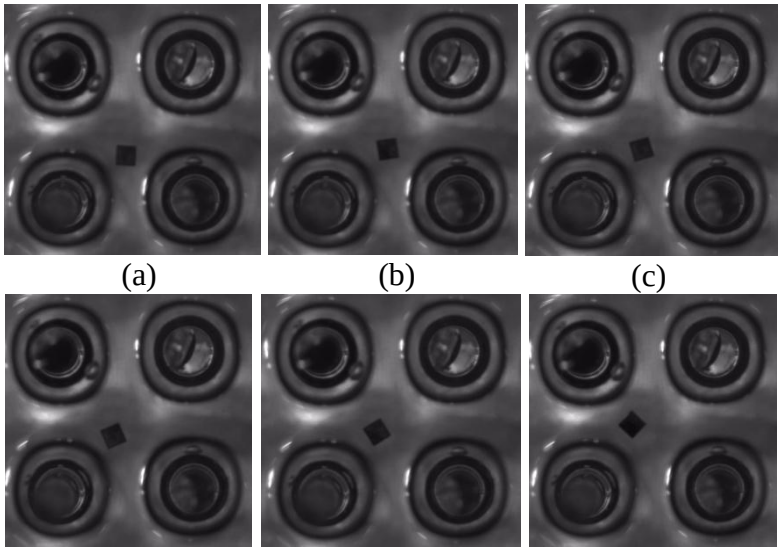

Figure 5.9: Top view of micropart between hydrophilic rods with 2.1 mm rod spacing. The micropart rotates about its z-axis as it reaches an equilibrium distance. Pictures show position at (a) 2.5 s, (b) 3.5 s, (c) 4.5 s, (d) 5.5 s, (e) 6.5 s, and (f) 12 s.

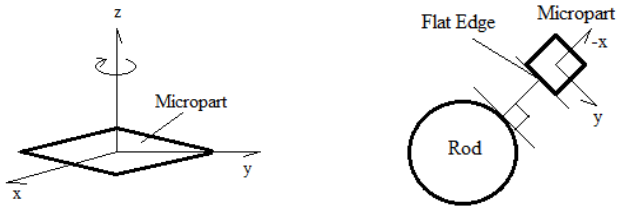

Figure 5.10: Micropart spins about its z-axis until it orients a flat edge to face the rod.

As shown in the graph in Figure 5.8, in the trials using hydrophobic rods, the microparts find an equilibrium distance immediately. The direction of the microparts

after placement onto the interface does not show a trend, nor is there a trend in reorientation of the micropart about its z-axis.

For both types of rods, the micropart does not get closer than 1 mm away from the outside diameter of its closest rod.

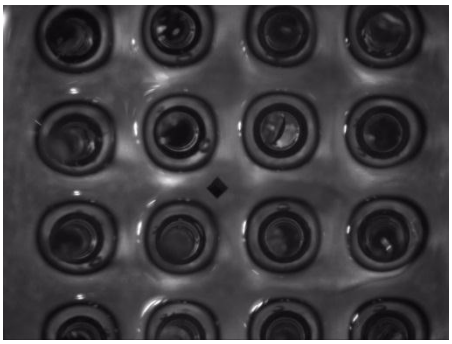

Figure 5.11: Wide top view of hydrophobic micropart among hydrophilic rods. The micropart stays more than 1 mm away from the rod's outside radius.

The separation distance between the micropart and closest rod for the next rod spacing is graphed in Figure 5.12.

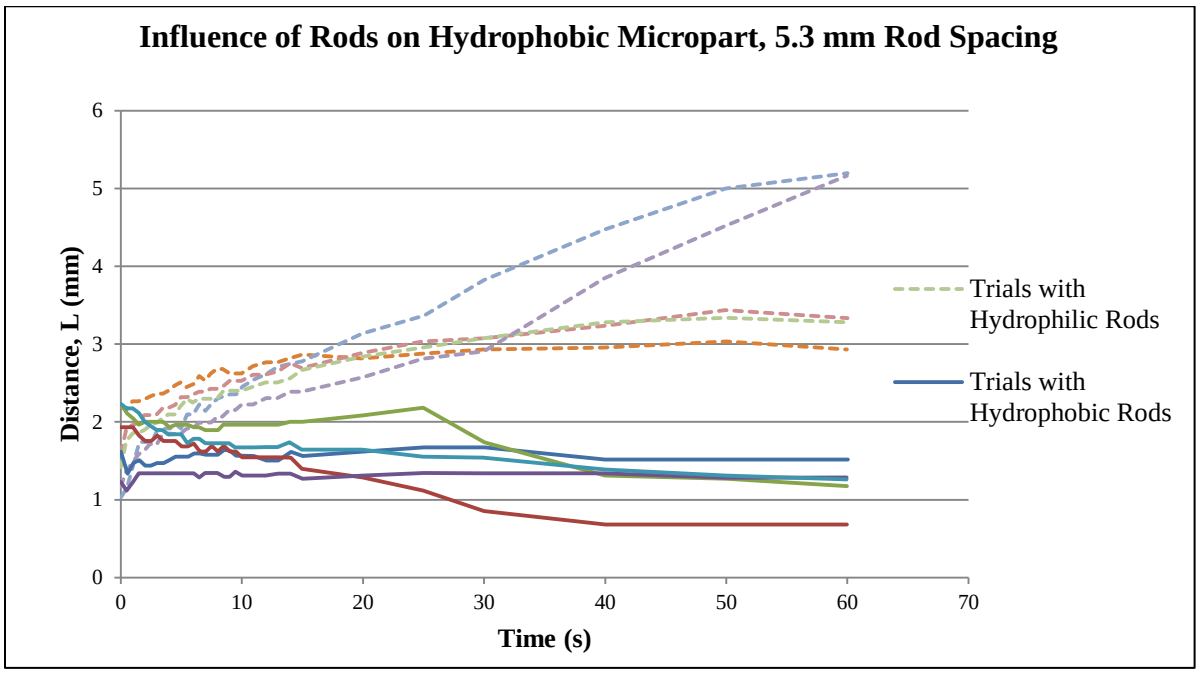

Figure 5.12: Graph of 5.3 mm rod spacing. Hydrophobic part with both hydrophilic and hydrophobic rods.

The slightly larger rod spacing allows for a slight trend to emerge in the direction of the micropart. In trials where hydrophilic rods are used, the micropart shifts away from the rod that it is placed nearest to. In only two trials do the microparts appear to reorient themselves to align an edge perpendicular to the rod as it moves away. Little rotation of the micropart takes place overall.

In trials where hydrophobic rods are present, the microparts initially oscillate in direction after initial deposition onto the interface, but overall there is little change in separation distance to the rod. In four of the five trials, the micropart finds an equilibrium position at a distance of approximately 1.3 mm from the outside diameter of the rod. In the fifth trial, the micropart gets no closer to the rod than 0.68 mm. There is little rotation of the micropart about its z-axis. In three of the five trials, an edge of the micropart faces the closest rod as it travels. One of these trials is pictured in Figure 5.13 below.

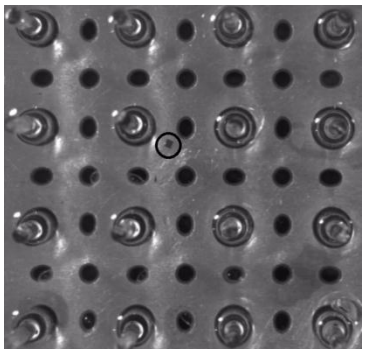

Figure 5.13: Top view of micropart between hydrophilic rods with 5.3 mm rod spacing. The micropart orients itself so that an edge faces the rods and stays more than 1 mm away from the rod's outside radius. The micropart is denoted with a circle.

In the next rod spacing arrangement, the results graphed below show a more pronounced trend than in the previous trials (Figure 5.14).

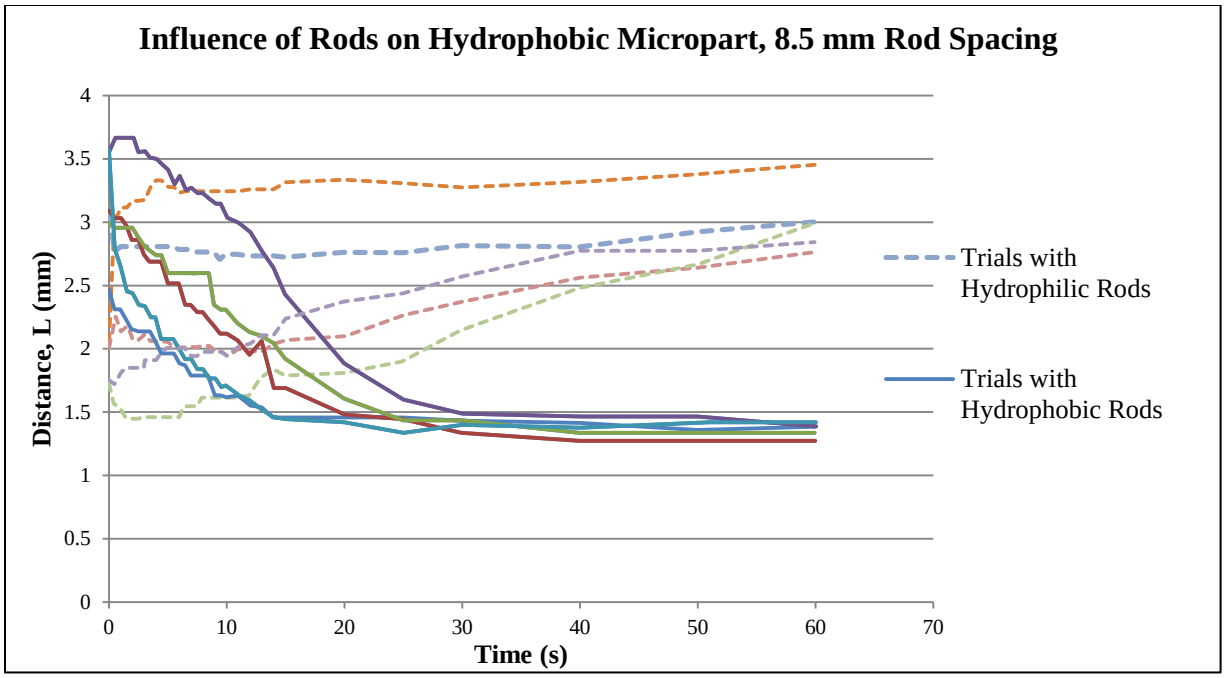

Figure 5.14: Graph of 8.5 mm rod spacing. Hydrophobic part with both hydrophilic and hydrophobic rods.

In four of the five trials in which the hydrophilic rods were present, the microparts complete the trial with a slightly larger separation distance from where they started. There is evidence of a slight trend of the microparts traveling away from the rod. There is very little reorientation of the microparts about its z-axis.

The microparts have a very pronounced trend in direction and in finding an equilibrium distance when in the presence of the hydrophobic rods. After deposition onto the interface, the separation distances of the microparts oscillate during the first fifteen seconds, but overall travel closer to their closest rod. This attractive overall direction is maintained until an equilibrium distance is reached. Approximately thirty seconds from the start of the trial, the microparts find an equilibrium distance of about 1.3 mm from the outside diameter of the rod. In all five trials, the micropart rotates immediately after deposition and faces an edge toward the rod that it is attracted to.

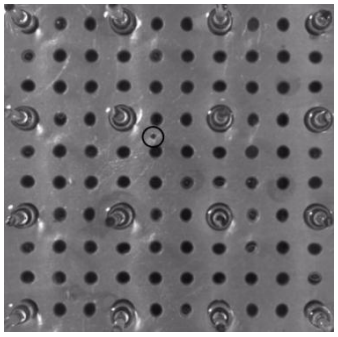

Figure 5.15: Top view of micropart between hydrophilic rods with 8.5 mm rod spacing. The micropart orients itself so that an edge faces the rods and stays about 1.3 mm away from the rod's outside radius. The micropart is denoted with a circle.

The separation distances of the trials exhibiting a rod spacing of 11.7 mm are graphed in Figure 5.16 below.

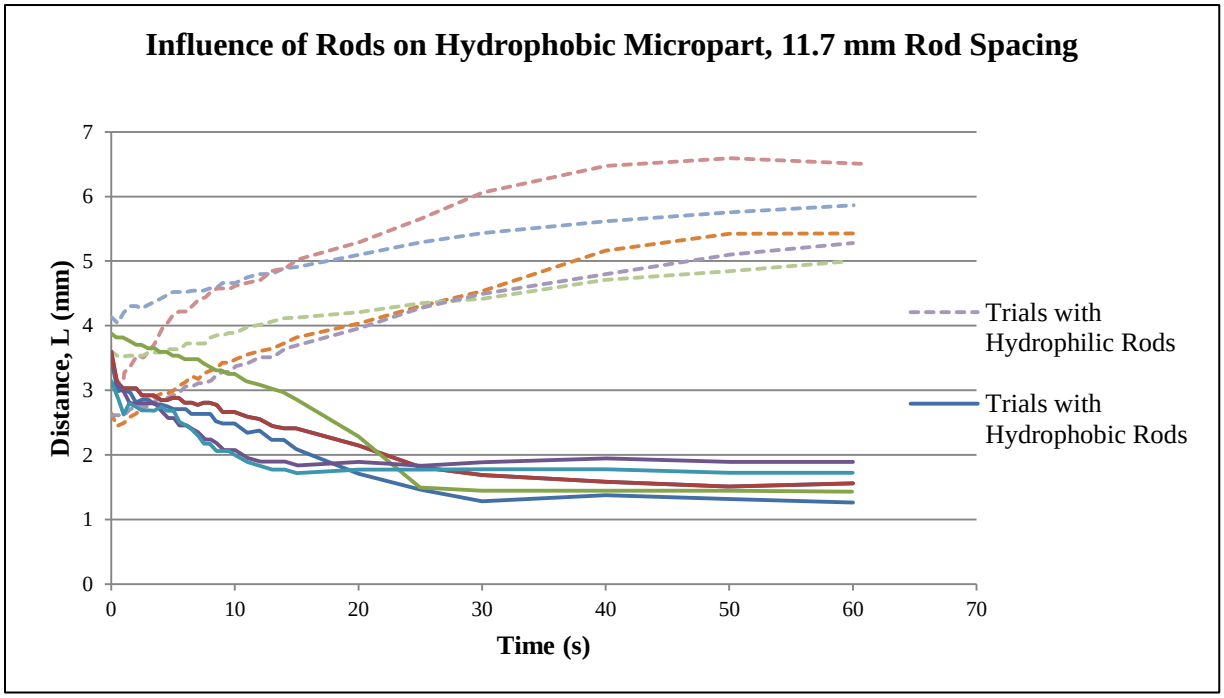

Figure 5.16: Graph of 11.7 mm rod spacing. Hydrophobic part with both hydrophilic and hydrophobic rods.

The microparts maintain the trend of traveling away from the hydrophilic rod. This is expected as the micropart is hydrophobic and the rod is hydrophilic. There is no pattern in the orientation of the microparts.

The microparts have a definite trend of moving toward the hydrophobic rod and reach an equilibrium distance of approximately 1.2 to 1.9 mm (Figure 5.17). In four of the five trials, the micropart keeps an edge facing the closest rod soon after deposition and through the end of the trial. In the fifth trial, the micropart does not rotate until about thirty seconds into the trial where it then spins to allow an edge to face the rod. It is inferred that this micropart reorientation is preferred.

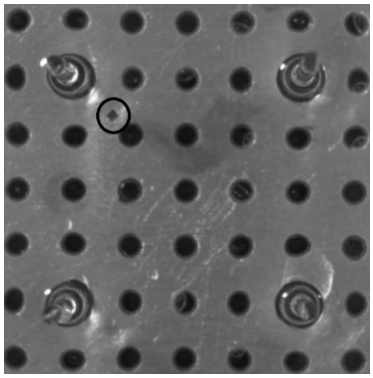

Figure 5.17: Top view of micropart between hydrophilic rods with 11.7 mm rod spacing. The micropart orients itself so that an edge faces the rods and stays 1.2 to 1.9 mm away from the rod's outside radius. The micropart is denoted with a circle.

In Figure 5.18, the separation distance is graphed for the final, largest rod spacing.

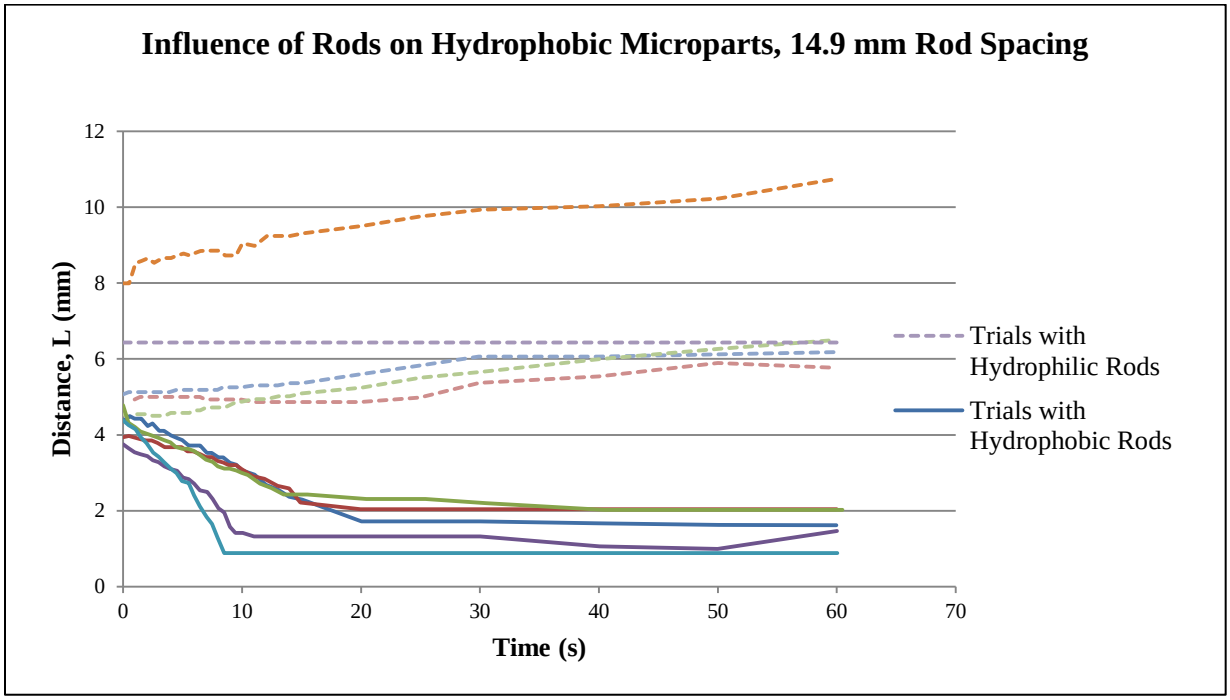

Figure 5.18: Graph of 14.9 mm rod spacing. Hydrophobic part with both hydrophilic and hydrophobic rods.

Overall, the microparts exhibit little change in separation distance from the hydrophilic rods after placement onto the interface. There is no noticeable pattern in the orientation of the micropart during travel and only some rotation takes place.

There is an obvious trend in the direction of travel for the microparts, given their apparent attraction to the hydrophobic rod. The equilibrium distance that the micropart reaches falls in a larger range than in the previous two trials. In this last subset of trials, the equilibrium distance ranges from 0.88 to 2.04 mm. In all five trials, the micropart reorients itself to allow an edge to face the closest rod and the micropart travels in the direction perpendicular to the edge facing the rod.

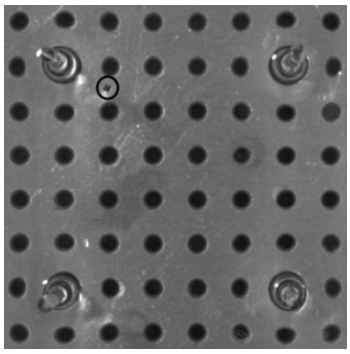

Figure 5.19: Top view of micropart between hydrophilic rods with 14.9 mm rod spacing. The micropart orients itself so that an edge faces the rods and stays 0.88 to 2.04 mm away from the rod's outside radius. The micropart is denoted with a circle.

5.1.1 Summary: Influence of Hydrophilic Rods on Hydrophobic Micropart

In the trials where microparts are tested against hydrophilic rods, the microparts travel away from the rods for the second, third and fourth spacing arrangements. It is expected that the microparts would appear to repel from the rods as the lateral capillary forces between two bodies that deform an interface in opposite direction push the two bodies apart. It is theorized that since the rods are hydrophilic and the microparts are hydrophobic, this state of opposing forces is partly responsible for the behavior of the microparts. Additionally, it is presumed that the microparts experience a gravitational pull toward the lower height of the interface located between the rods. Gravity is another dominating contributing factor to the movement of the microparts.

It is surmised that this behavior does not occur for the first rod spacing arrangement because there is no flat portion of the interface for this configuration. When the floating microparts are repelled by the semi-immersed bodies, they travel to a flatter region of the interface where they are in a more equilibrium state. It requires less energy for the micropart to lay on a flat interface at a lower vertical height. This flat region of

minimal energy is not present in the first spacing arrangement and there is no apparent trend in the direction of the micropart.

In the fifth spacing arrangement, only a slight trend of directional movement away from the rod occurs, but there is overall little movement of the microparts. It is assumed that the greater distance between the closest rod and the micropart at the initial placement location is too large for the deformation caused by the rod to have a highly noticeable effect on the behavior of the micropart.

The strongest trend occurs for the fourth rod spacing arrangement in trials where hydrophilic rods are used. This rod spacing seems to have the most repeatable results as the microparts travel away from the rod.

In the first spacing arrangement, the micropart orients itself to have an edge face the closest rod. This does not occur in the other four, larger spacing arrangements. In the smallest rod spacing, the curvature created by all four rods in close proximity influences the micropart in all directions, causing this orientation. More is discussed about micropart orientation in the next section of this chapter.

5.1.2 Summary: Influence of Hydrophobic Rods on Hydrophobic Micropart

Overall, in the trials where microparts are tested against hydrophobic rods, the microparts exhibit a behavioral pattern where they travel toward the rod in the third, fourth and fifth rod spacing arrangements. The microparts stop at an equilibrium distance that is similar in all of the twenty-five trials; approximately 1 to 2 mm away from the outside perimeter of the rod. The following graph shows the final distance from the rod reached by the micropart in each trial. The middle rod spacing brings the most repeatable results.

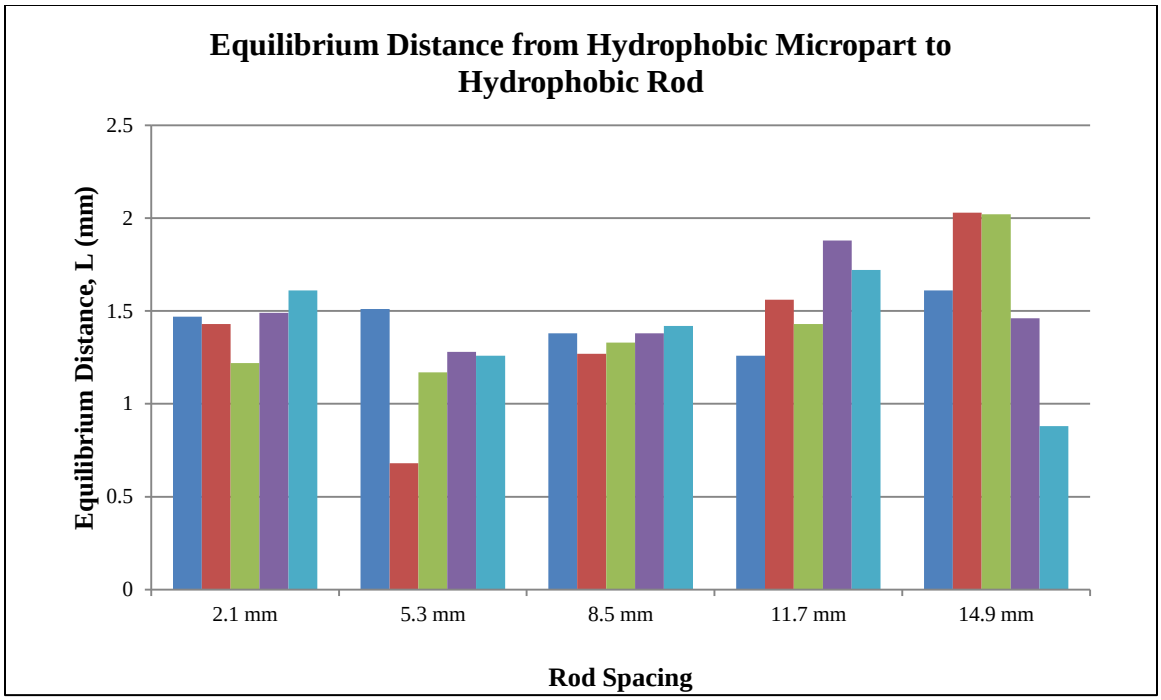

Figure 5.20: Graph of equilibrium distance reached from hydrophobic microparts to hydrophobic rod for all rod spacing arrangements.

These results are indicative of more happening on the interface that is responsible for the movement of the micropart than just lateral capillary forces. The fact that there is an equilibrium position requires the presence of a balancing force that is not included in the simple model discussed in Chapter 2. The figures below show a micropart that has traveled toward a hydrophobic rod and then reached an equilibrium distance. Figure 5.21 shows a close view and the interfaces are labeled for clarification. Figure 5.22 captures a micropart that maintains an equilibrium separation distance while spinning around the hydrophobic rod and keeping a flat edge facing the rod.

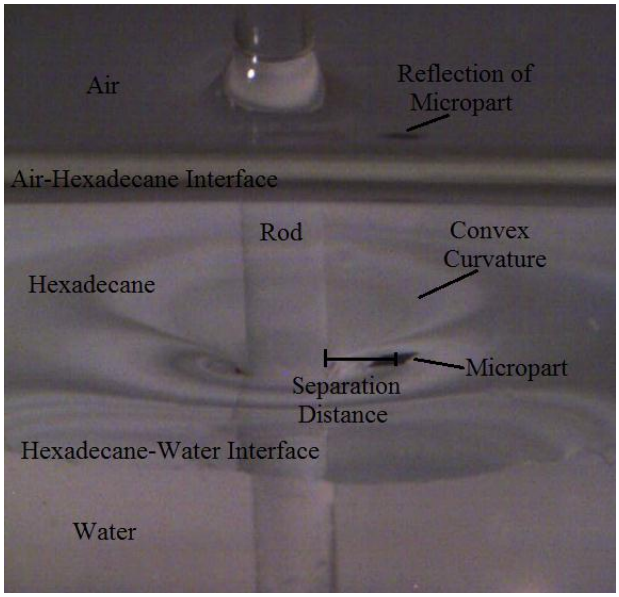

Figure 5.21: Picture of micropart floating on hexadecane-water interface. The hydrophobic vertical rod forms a convex shape of the hexadecane-water interface. The air-hexadecane interface is also visible. The separation distance between the midpoint of the micropart and the outside diameter of the rod is labeled. Notice the reflection of the micropart on the air-hexadecane interface.

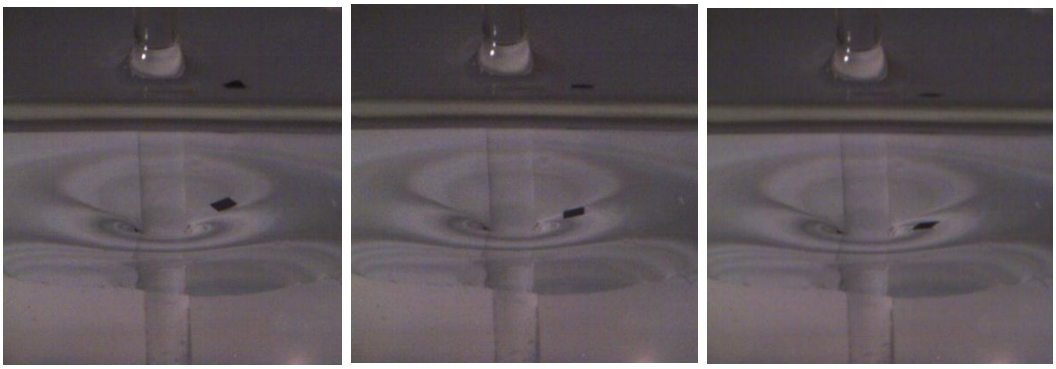

Figure 5.22: Close view of micropart on hexadecane-water interface.

It is expected that the hydrophobic microparts would travel to the hydrophobic rod since they both deform the interface in the same direction. Two bodies that are both hydrophobic or both hydrophilic tend to cluster on an interface per the description of lateral capillary forces. This means that two bodies that deform the interface in the same direction will travel toward each other until they touch. Once they reach each other, they tend to stick together, side by side on the interface. By assuming this reasoning, it is

expected that that the hydrophobic microparts would travel all the way to the rod until they touch it and then cluster against it. Instead, though, an equilibrium separation distance is reached away from the rod and then maintained.

About the hydrophobic rods, the interface is a convex shape where the central region of the interface between rods is higher than the interface immediately touching the rod. Perhaps the micropart travels toward the rod to reach a lower height on the interface. As in the case with hydrophilic rods, the micropart tends to travel to a lower vertical location. This may be due to the gravitational pull on the part that causes it to travel down the sloped interface. This could allow for the part to be located at a position where a minimum potential energy is present.

The curvature of the interface surrounding the rods, though, allows the microparts to only travel to a certain distance away from its center. From the pictures displayed in Figures 5.21 and 5.22, it appears that the equilibrium distance for the micropart is located right outside of where the curvature of the interface is the greatest. As mentioned in Chapter 2, where the curvature of an interface increases, the surface area increases and there is more energy present at that location. Perhaps the interface at the position where there is greater energy repels the micropart, causing it to stop moving toward the rod. The micropart stays at a location where there is minimal energy.

An additional assumption can be made as to why it requires more energy for the micropart to be in this position of greater curvature. As the micropart floats anywhere on the interface, it slightly deforms the interface and a small volume of fluid is displaced. The greater the curvature is at the location of the micropart, the more of the interface that is deformed to support the floating micropart and the more fluid volume that is displaced.

The increased surface area allows for more energy to be present at the surface while the fluid volume is conserved. The micropart may avoid a higher curvature of the interface to avoid this higher energy state that would be required to keep it floating at a location of increased curvature. Figure 5.23 describes this situation of increased displacement of volume.

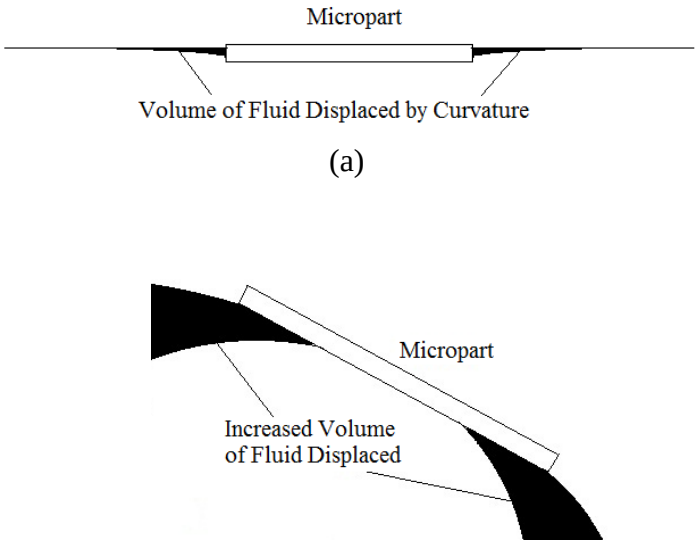

Figure 5.23: Black shaded areas depict volume of fluid displaced by a floating micropart on an interface. (a) Little curvature and (b) increased curvature.

An additional theory suggests that at the location of the equilibrium separation distance, the lateral capillary forces change direction and are in the opposite direction as the lateral capillary forces further away from the rod. Perhaps the forces converge at this diameter about the rod where the micropart stops, trapping the micropart at this distance.

There is little movement by the microparts in the first and second spacing arrangements. It is concluded that the deposition location is too close to the equilibrium separation distance for the microparts to undergo too much movement.

The third spacing arrangement shows the strongest trend with the parts all stopping at a similar distance of approximately 1.3 mm across all five trials. It is noted for consideration of future trials that this rod spacing produces the most repeatable results.

When traveling to a hydrophobic rod, the micropart spins to have a leading edge face the rod in the latter four spacing arrangements, but not in the first. When the micropart is attracted to the rod, it travels in the direction approximately perpendicular to the leading edge of the micropart, facing the rod as shown in Figure 5.24.

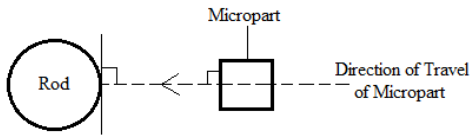

Figure 5.24: Leading edge of micropart traveling to rod. The direction of travel is perpendicular to the leading edge. The leading edge is parallel to the tangent of the location on the rod diameter that is in line with the direction of travel.

As mentioned, this is not the case in the latter four spacing arrangements where hydrophilic rods are used. Perhaps this occurs when there is attraction to the rod and not repulsion from the rod because the attractive force is more directional. It is assumed that the curvature created by a hydrophobic rod causes the micropart to travel to a concentrated destination (Figure 5.25(a)). A micropart being repulsed travels to a less specific location, instead, to a general region away from the rod (Figure 5.25(b)). Because the direction of the part is less specific, the part does not rotate to a specific orientation. This rotation does not take place in the smallest spacing arrangement of the hydrophobic rods because little distance is traveled by the micropart in these trials.

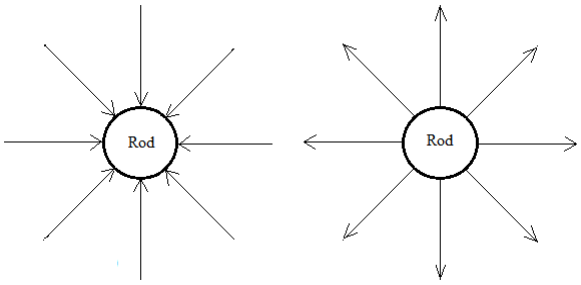

Figure 5.25: Direction of micropart travel. Travel is (a) more specific when micropart is attracted toward the rod and (b) less specific when micropart is repelled from rod.

In all of the cases where the micropart rotates to orient so that an edge can face the rod, little rotation actually takes place. The part spins in a direction that allows the closest edge to face the rod. Because of the square geometry of the part, this spin is at most 45 degrees, or half of 90 degrees (Figure 5.26).

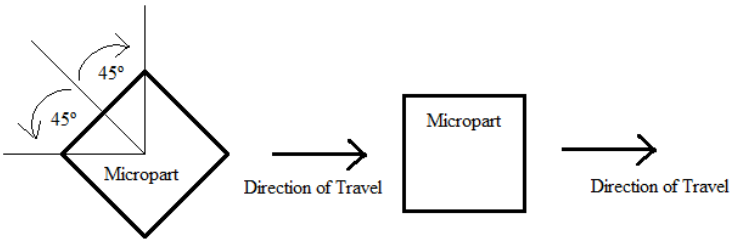

Figure 5.26: Maximum angle micropart must spin to get a leading edge to face perpendicular to direction of travel.

Once a part reaches its equilibrium distance, it may rotate around the rod, maintaining the same distance from the rod and keeping the same edge facing the rod (Figure 5.27).

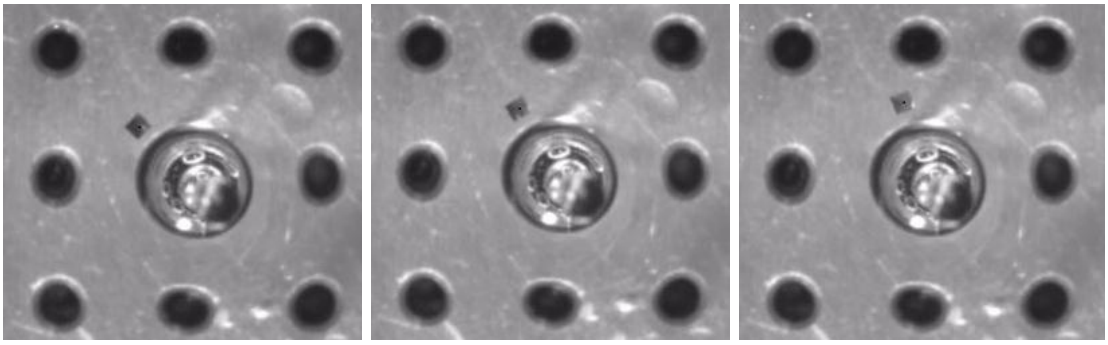

(a) (b) (c)

Figure 5.27: Picture of micropart circling a rod after reaching its equilibrium distance. The same edge of micropart faces the rod after equilibrium distance is met and maintained. Pictures show (a) 30 s, (b) 40 s and (c) 50 s into trial.

Overall, there is evidence to suggest that the attractive force is stronger than the repulsive force. In the trials where hydrophobic rods are used and there is a trend for the microparts to be attracted toward the rod, the microparts reach an equilibrium position faster and travel a greater distance in a shorter time. In the trials where hydrophilic rods or present, the microparts move slower and continue to move away from the rod throughout the entire trial. This is indicative of a less specific directional repulsive force and a stronger, more concentrated attractive force.

5.2 Hydrophilic vs. Hydrophobic Rods: Influence on Hydrophilic Micropart

To further test the attractive and repulsive relationship between the rods and the microparts, a second set of trials is conducted using hydrophilic microparts instead of hydrophobic microparts. The third spacing arrangement that exhibited the strongest trend in the previous set of trials is used for both hydrophilic and hydrophobic rods. In all of the trials, the micropart is deposited one quarter of the distance between diagonal rods as in the previous trials.

The following table lists the trials conducted in the second set of the experiment.

Table 5.2: List of second set of trials. Hydrophilic and hydrophobic rods for 8.5 mm spacing arrangements using hydrophilic microparts

Hydrophilic Microparts	
Hydrophilic Rods	Hydrophobic Rods
8.5 mm Rod Spacing/12.44 mm Diag. (5 Trials)	8.5 mm Rod Spacing/12.44 mm Diag. (5 Trials)

The microparts were treated to become hydrophilic by placing them in hydrogen peroxide 30% by weight in water and left to sit for one hour. Afterwards they were rinsed and then stored in deionized water. The microparts were tested to ensure that they were hydrophilic by placing a sample of them on an air-water interface with other hydrophobic microparts. The hydrophilic microparts clustered together and repelled away from the hydrophobic microparts. This served as evidence that they were properly rendered hydrophilic.

The following graph documents the separation distance between the micropart and its closest rod for an 8.5 mm rod spacing using both hydrophilic and hydrophobic rods.

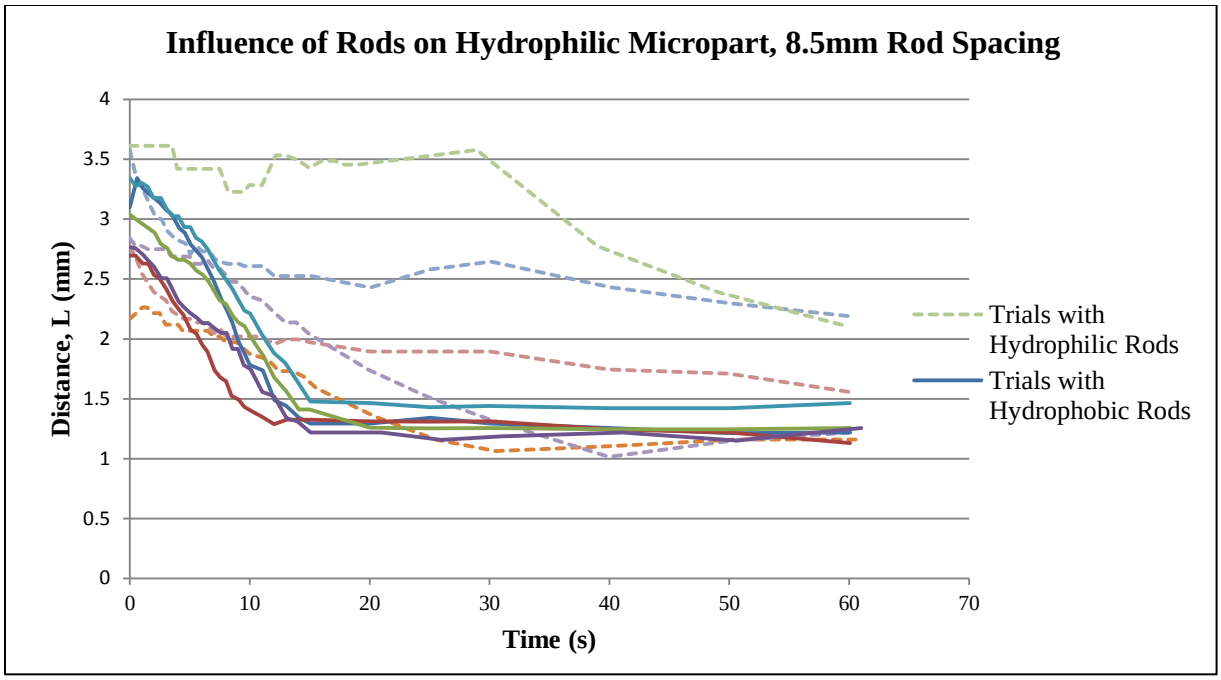

Figure 5.28: Graph of 8.5 mm rod spacing with hydrophilic microparts. Both hydrophilic and hydrophobic rods are used in separate trials.

Overall, both hydrophilic and hydrophobic rods attract the hydrophilic microparts. The trend of attraction to the hydrophobic rods is much stronger and the microparts find an equilibrium separation distance early in the trials, approximately 1.1 to 1.5 mm away from the outside diameter of the closest rod. The microparts tested with the hydrophobic rods move with a higher velocity. This signifies a stronger lateral attractive force that has a concentrated direction. It is expected that the hydrophilic microparts would attract toward the hydrophilic rods since they deform the interface in the same direction.

The hydrophilic microparts are also attracted to the hydrophobic rods in spite of the different directions in interface deformations that they cause. This may be for the same reason that the hydrophobic microparts were attracted to the hydrophobic rods in the previous set of trials. As discussed, the microparts may travel to a lower height on the interface due to a gravitational pull. The shape of the interface created by the

hydrophobic rod has such curvature that the micropart travels down its hill-like shape. In two of the trials, the hydrophilic microparts seem to reach an equilibrium separation distance similar to that reached by the hydrophobic microparts. In the other three trials, the micropart is still in motion at the end of the sixty seconds. Had more time elapsed, it is possible that they, too, may have reached a similar equilibrium distance.

The hydrophobic rods and the hydrophilic parts deform the hexadecane-water interface in different directions, so it is expected that the lateral capillary forces present would repel each other and the microparts would travel away from the rods. This suggests that perhaps the interface deformation criteria of attraction and repulsion are not the dominating factor contributing to the behavior of the microparts as expected. Perhaps it is gravity, instead of the lateral capillary forces, that is the dominating contributor to the behavior of the microparts until they reach their equilibrium distance.

In all of the trials using hydrophobic rods, the microparts orient themselves to have an edge facing the rod. There is no noticeable trend in orientation in the trials using hydrophilic rods. It is assumed that this happens in response to a stronger attraction toward hydrophobic rods than hydrophilic rods. The extreme curvature of the convex interface caused by the hydrophobic rods is more influential on the movement of the micropart than the same interface deformation direction caused by the hydrophilic rods.

5.3 Hydrophilic and Hydrophobic Rods: Influence on Hydrophilic and Hydrophobic Microparts Placed Close to the Rod

The phenomenon that the microparts reach an equilibrium separation distance away from the rod is an interesting event. In all of the trials conducted thus far, the micropart is placed a distance away from the rod and allowed to travel toward the rod

before reaching the equilibrium separation distance. A third set of trials is conducted to observe the behavior of the microparts when they are deposited closer to the rod, interacting within or close to the distance where the slope of the interface dramatically increases. Using the same rod spacing as was used in the previous set of trials, the microparts are deposited onto the interface at about 0.5 to 2.3 mm from the rod, an approximate expected equilibrium distance. The following table lists the third set of trials performed.

Table 5.3: List of third set of trials. Hydrophilic and hydrophobic rods for 8.5 mm spacing arrangements using hydrophilic and hydrophobic microparts

Hydrophilic Microparts	
Hydrophilic Rods	Hydrophobic Rods
8.5 mm Rod Spacing/12.44 mm Diag. (5 Trials)	8.5 mm Rod Spacing/12.44 mm Diag. (5 Trials)
Hydrophobic Microparts	
Hydrophilic Rods	Hydrophobic Rods
8.5 mm Rod Spacing/12.44 mm Diag. (5 Trials)	8.5 mm Rod Spacing/12.44 mm Diag. (5 Trials)

The micropart is deposited close to the rod in all trials, as pictured in Figure 5.29.

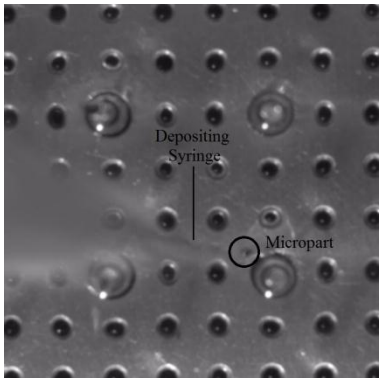

Figure 5.29: Picture of micropart deposition close to rod. Micropart is denoted with a circle.

The following graph depicts the distance from the micropart to the closest rod versus time for both hydrophilic and hydrophobic microparts, and both hydrophilic and hydrophobic rods.

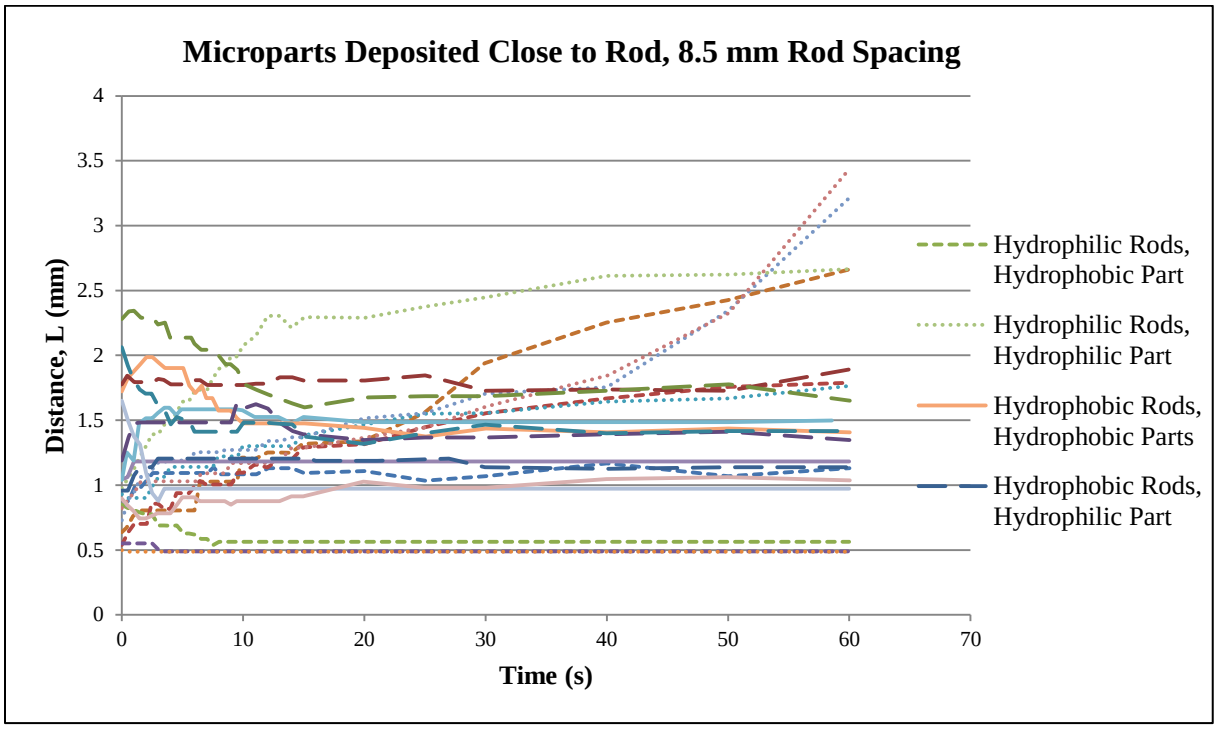

Figure 5.30: Graph of 8.5 mm rod spacing with both hydrophilic and hydrophobic rods with both hydrophilic and hydrophobic parts deposited close.

There is no decipherable trend for the trials using hydrophilic rods and hydrophobic microparts. For the trials using hydrophilic rods and hydrophilic microparts, there is a slight trend for the microparts to travel slightly away from the rod. In all of the trials using hydrophobic rods, the microparts generally do not travel in a direction away or toward the rod, but instead have very little movement overall.

The slight trend for the trials using hydrophilic rods and hydrophilic microparts is not strong enough to make an assumption of causality. Per the explanation of lateral capillary forces, it would be expected that because both bodies are hydrophilic, they would attract towards each other or maintain the distance from the rods at which they

were deposited. The hydrophilic rods create a positive meniscus slope at the rod. Perhaps the microparts in these trials were placed high enough on the slope to have enough momentum to travel down the interface in search of a flatter surface and a lower energy state away from the rods.

In all of the trials with hydrophobic rods, the microparts reach a distance of 1 to 1.8 mm from the rod and make little change in this separation distance for the remainder of the trial. Because little directional movement takes place, it is surmised that the close placement of the microparts to what is considered to be an equilibrium distance from the hydrophobic rods allows for little overall displacement of the micropart. The micropart is subject to the governing physics that determines the equilibrium distance even if the micropart is deposited close to the hydrophobic rod. In all of the trials, none of the rods fall all the way down the convex curvature of the interface and reach the rod. This suggests that even if the micropart is placed closer to the rod than its equilibrium distance, it will still be subject to this equilibrium distance and perhaps travel away from the rod to reach it.

Regarding the orientation of the micropart, a flat edge of the micropart tends to face the rod in the majority of the trials except for the trial using hydrophilic rods with the hydrophilic microparts, where no trend is apparent. The close proximity of the micropart to the rod could be responsible for this reorientation. In all incidences where the micropart maintains an equilibrium distance while swinging around the rod (as discussed earlier in regard to Figure 5.27), it keeps one edge facing the rod as it sweeps.

5.4 Hydrophilic and Hydrophobic Plates: Hydrophilic and Hydrophobic Microparts Deposited Away from and Close to the Plate

So far it has been established that a micropart reaches an equilibrium distance away from the outside diameter of the hydrophobic rod, regardless of whether the micropart is placed close to or away from the rod. The aim of the fourth and fifth sets of trials is to observe if this equilibrium separation distance is created by the geometry of the curvature created by the cylindrical rod, or if another convexly shaped interface produces an equilibrium separation distance that the microparts travel to. The next two sets of trials implement a glass plate that deforms the hexadecane-water interface instead of the quartz rods. A planar surface created by a plate contains one finite radius of curvature. The rods create a surface that has two radii of curvature, allowing for the potential to create competing forces. The fourth set of trials tests a hydrophilic plate while introducing hydrophilic and hydrophobic microparts placed away from and close to the plate. These trials serve to determine if there is an attractive or repulsive relationship between a hydrophilic plate and the microparts. Table 5.4 lists the trials conducted and Figure 5.31 depicts the hexadecane-water interface in the presence of a hydrophilic plate.

Table 5.4: List of fourth set of trials. Hydrophilic plate using hydrophilic and hydrophobic microparts deposited away from and close to Plate

Hydrophilic Plate	
Hydrophilic Microparts	Hydrophobic Microparts
Deposited Away from Plate (5 Trials)	Deposited Away from Plate (5 Trials)
Deposited Close to Plate (5 Trials)	Deposited Close to Plate (5 Trials)

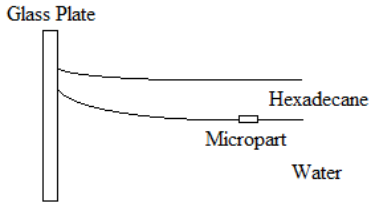

Figure 5.31: Micropart placed on a hexadecane-water interface away from a hydrophilic plate.

The fifth set of trials uses a hydrophobic plate. The purpose of this set of trials is to observe whether the same behavior is created by the convex shape introduced by the plate as that which occurs when hydrophobic rods are present. Table 5.5 lists the fifth set of trials and Figure 5.32 depicts the hexadecane-water interface in the presence of a hydrophobic plate.

Table 5.5: List of fifth set of trials. Hydrophobic plate using hydrophilic and hydrophobic microparts deposited away from and close to plate

Hydrophobic Plate	
Hydrophilic Microparts	Hydrophobic Microparts
Deposited Away from Plate (5 Trials)	Deposited Away from Plate (5 Trials)
Deposited Close to Plate (5 Trials)	Deposited Close to Plate (5 Trials)

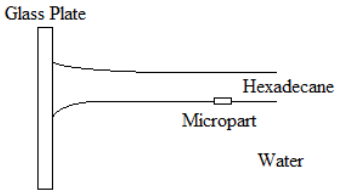

Figure 5.32: Micropart placed on a hexadecane-water interface away from a hydrophobic plate.

In the trials where deposition takes place close to the plate, the micropart is deposited at about 1.6 to 3.6 mm away from the plate (Figure 5.33). This distance reflects a similar spacing to the deposition distance used in the second set of trials.

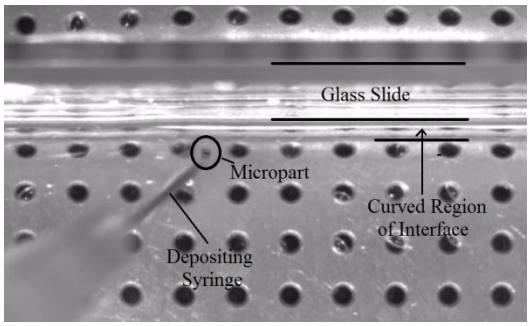

Figure 5.33: Picture of micropart deposited close to hydrophobic glass plate.

In trials where the micropart is deposited away from the rod, a contrasting deposition distance of about 6.7 to 10 mm away from the plate is used for comparison (Figure 5.34).

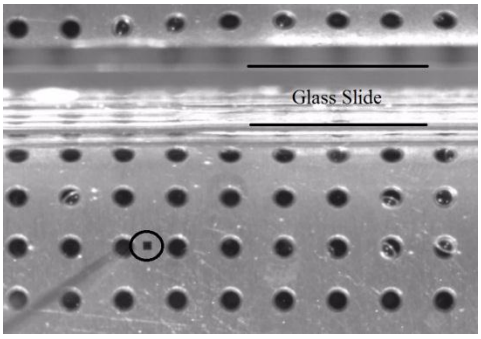

Figure 5.34: Picture of micropart deposited away from hydrophobic glass plate.

The following graph displays the separation distance of the micropart versus time with the use of a hydrophilic plate.

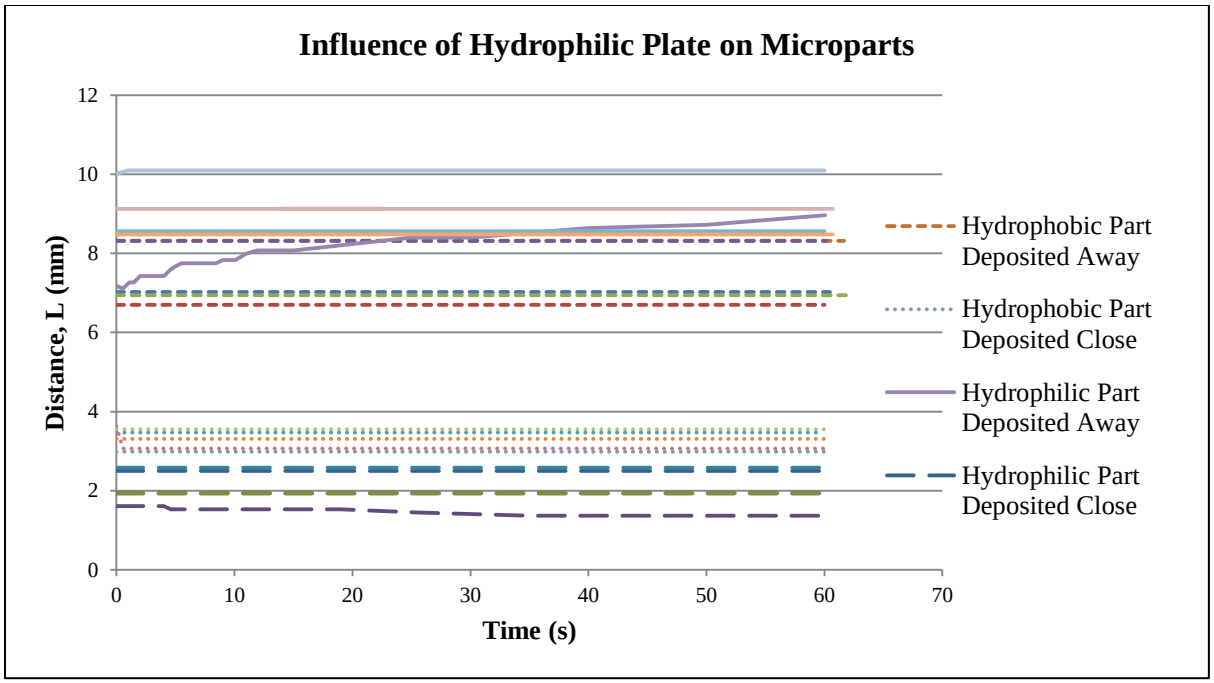

Figure 5.35: Graph of hydrophilic plate. Both hydrophobic and hydrophilic microparts deposited away from and close to plate.

In nineteen of the twenty trials conducted, there is almost no movement made by the micropart after being deposited either close to or away from the hydrophilic plate. This includes both hydrophilic and hydrophobic parts. In every trial conducted, there is no rotation of the micropart about its z-axis. These results are evidence for the assumption that the presence of the hydrophilic plate has no influence on either hydrophilic or hydrophobic parts.

The following graph displays the separation distance for the fifth set of trials where a hydrophobic plate is present.

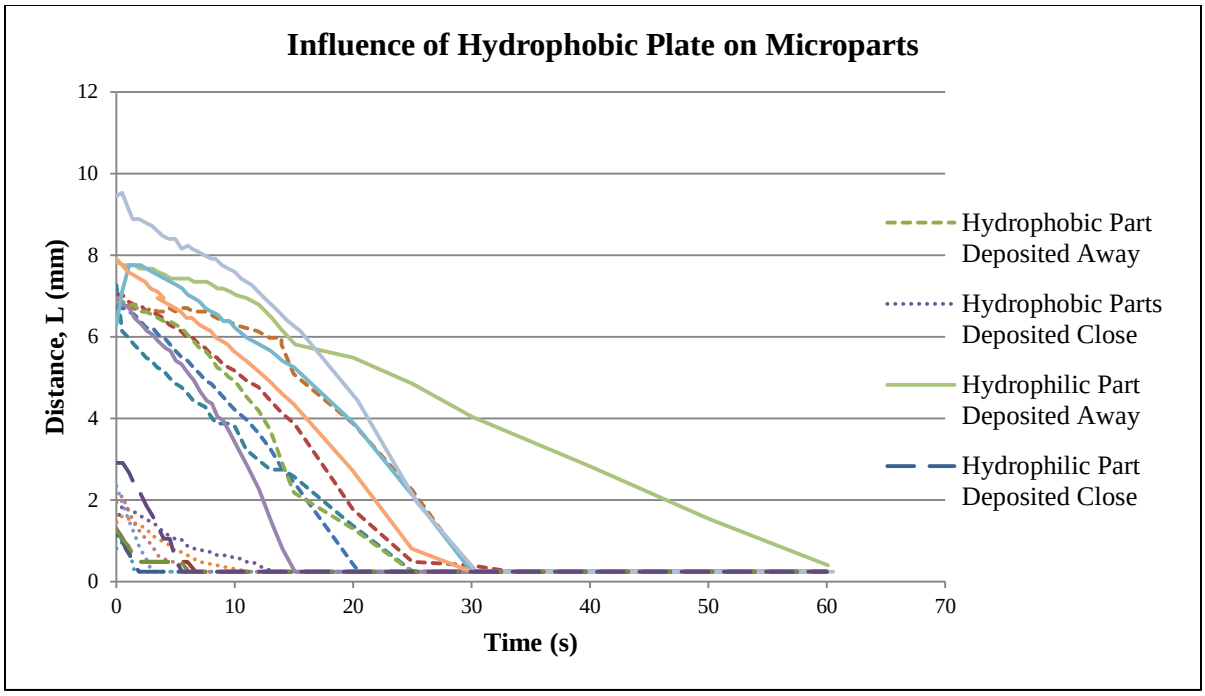

Figure 5.36: Graph of hydrophobic plate. Both hydrophobic and hydrophilic microparts deposited away from and close to plate.

In every trial conducted, the micropart is attracted to the hydrophobic plate. Attraction occurs when the micropart is hydrophilic, hydrophobic, placed close to the plate, or placed away from the plate. It is speculated that this occurs because the microparts travel to a lower height on the interface at a location of minimum potential energy. The dominating force responsible for this direction in motion is gravity. The interfacial deformation direction does not appear to be the main contributing factor to the behavior of the micropart.

In the previous sets of trials, the overall trend is that both hydrophilic and hydrophobic microparts travel to a hydrophobic rod. This is also the case with the hydrophobic plate. The major difference is that the microparts maintain an equilibrium separation distance away from the rods. In the trials where a hydrophobic plate is used, the microparts travel all to the way to the surface of the plate and the equilibrium position

is against the plate. The graph in Figure 5.36 shows the micropart stopping at a distance of 0.25 mm away from the surface of the plate. This is because the separation distance between the micropart and the plate is measured from the midpoint of the 0.5 mm wide micropart and the surface of the plate.

It is concluded that it is the geometry of the interface about the rod that creates an equilibrium position for the micropart. This influential curvature cannot be created by a flat surface such as a glass plate.

In the trials where a hydrophobic plate is present, there is very little or no rotation of the micropart about its z-axis. The micropart has no preference in orientation as it travels to the plate or when it reaches the plate. This means that an edge or a point of the micropart may make contact with the plate as it arrives. It seems that an interface may need two radii of curvature, as is the case with the interface created by the rods, in order for a micropart to undergo a specific orientation during travel.

5.5 Hydrophobic Rods: Influence on Different Sized Microparts

It has been concluded that there is a direct relationship between the geometry of the surface created by the presence of the rods and the existence of an equilibrium separation distance away from the rod. Perhaps the relationship involves the size of the micropart itself. The sixth set of trials conducted implements silicon microparts of two additional sizes among hydrophobic rods. The 8.5 mm rod spacing is used as it produced the most repeatable results, as exhibited in previous trials. Both larger and smaller microparts than the original 500 μm parts are used. The larger microparts are 1 mm x 1mm x 10 μm and the smaller microparts are 250 μm x 250 μm x 10 μm in dimension. The additional microparts have been fabricated with the same procedures as the 500 μm

part. They are also hydrophobic and have been treated with hydrofluoric acid to ensure their hydrophobicity. The following table lists the trials performed using these additional sizes.

Table 5.6: List of sixth set of trials. Hydrophobic rods using 1 mm and 250 μm hydrophobic parts

Hydrophobic Rod, 8.5mm Rod Spacing/12.44 mm Diagonal Spacing
1 mm Hydrophobic Part (5 Trials)
250 μm Hydrophobic Part (5 Trials)

The trials are conducted in the same manner as the first and second set of trials. The microparts are deposited on the hexadecane-water interface at a location approximately one quarter of the distance between diagonal rods (Figure 5.37). Each trial implements a single micropart and tracks its separation distance from the rod for sixty seconds.

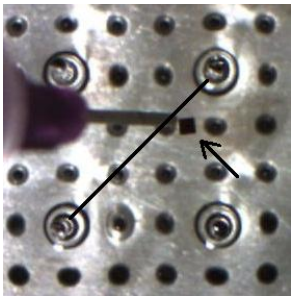

Figure 5.37: Placement of 1 mm micropart approximately one quarter of diagonal distance.

The following graph shows trials using all three sizes of hydrophobic microparts for a rod spacing of 8.5 mm. The data for the 500 μm parts is taken from the first set of trials described in section 5.1. The data is redisplayed in Figure 5.38 for comparison to the microparts of other sizes.

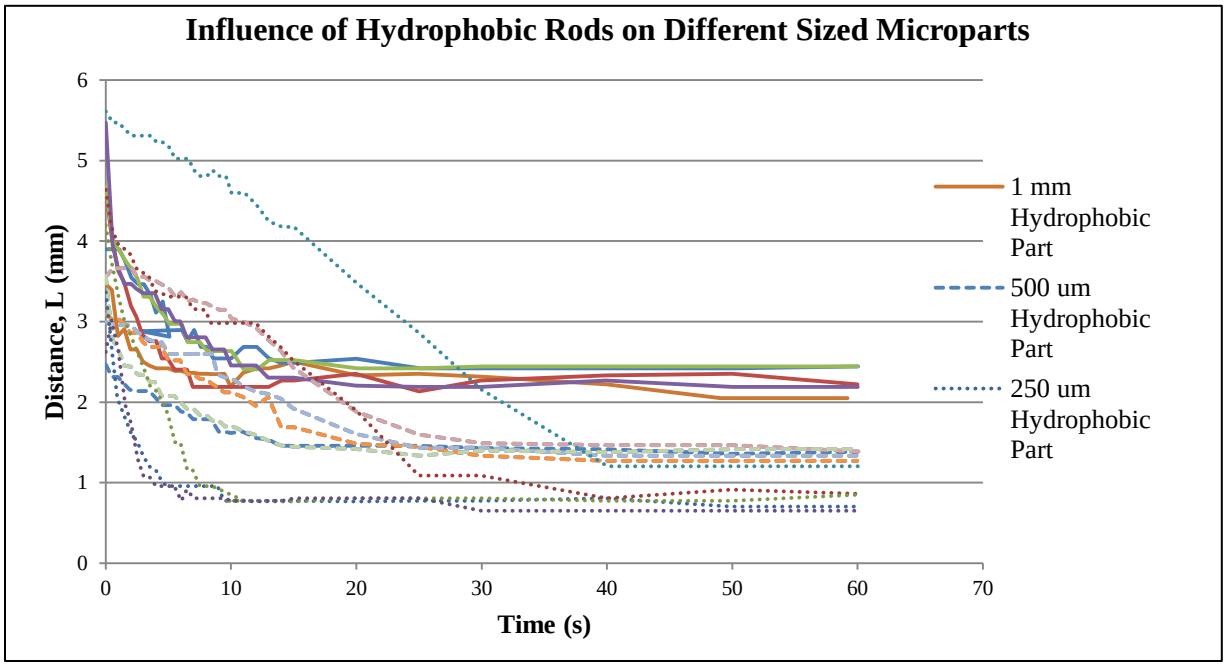

Figure 5.38: Graph of 8.5 mm rod spacing: hydrophilic rods with 1 mm, 500 µm and 250 µm parts.

In every subset of trials, there is a definite trend of the microparts reaching a similar equilibrium separation distance. For the 1 mm microparts, the equilibrium separation distance is about 2.3 mm. For the 500 µm and 250 µm parts, the equilibrium separation distance is about 1.3 mm and 0.85 mm, respectively. In all of the trials, the microparts also orient themselves during travel by spinning about their z-axis until a flat edge faces the rod. This reorientation takes the least amount of time for the 1 mm part and takes the most amount of time for the 250 µm part. The following pictures show a 1 mm part (Figure 5.39) and a 250 µm part (Figure 5.40) maintaining an equilibrium distance from the hydrophobic rod and spinning about it while keeping an edge facing the rod.

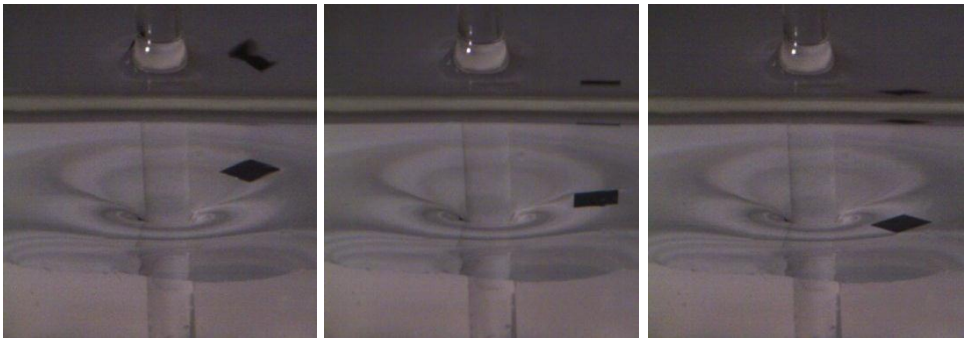

Figure 5.39: Pictures of 1 mm part spinning about hydrophobic rod at an equilibrium distance. Approximately 4 seconds elapsed between photos.

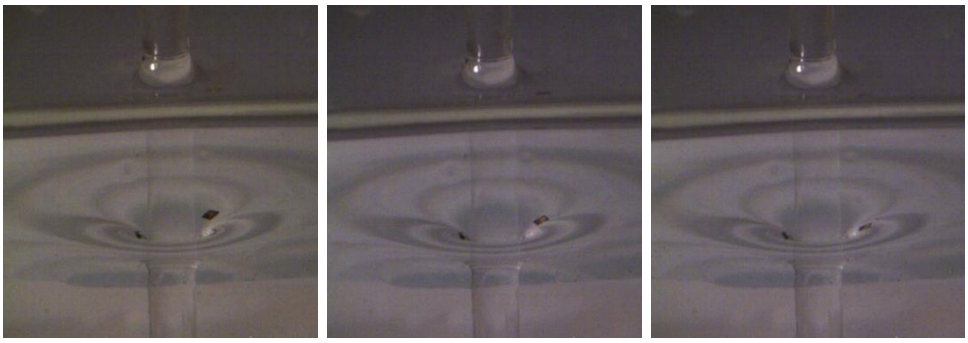

Figure 5.40: Pictures of a 250 μm part spinning about hydrophobic rod at an equilibrium distance. Approximately 4 seconds elapsed between photos.

The behavior of the larger and smaller microparts is the same as that for the 500 μm parts exhibited in the first set of trials. The explanation for this behavior is also surmised to be the same. The microparts travel to a location of minimal energy level by finding an equilibrium position at a lower height than which they were deposited. Movement of the microparts is dominated by the gravitational pull down the slope of the curvature of the interface. Movement stops before the micropart reaches the location on the interface where the curvature is the greatest and the energy is increased.

5.6 Larger Diameter Hydrophobic Rods: Influence on Different Sized Microparts

Determining that the equilibrium separation distance is created by the curvature of the interface deformed by a hydrophobic rod, an additional and final set of trials is

conducted with a slightly altered curvature. The last set of trials uses hydrophilic rods that have a diameter of 2 mm as opposed to 1 mm. All other parameters are kept the same as in the previous set of trials. Table 5.7 lists these trials.

Table 5.7: List of seventh set of trials. 2 mm diameter hydrophobic rods using 1mm, 500 µm and 250 µm hydrophobic parts

2 mm Diameter Hydrophobic Rod, 8.5mm Rod Spacing/12.44 mm Diagonal Spacing
1 mm Hydrophobic Part (5 Trials)
500 µm Hydrophobic Part (5 Trials)
250 µm Hydrophobic Part (5 Trials)

Figure 5.41 displays the results regarding the separation distance.

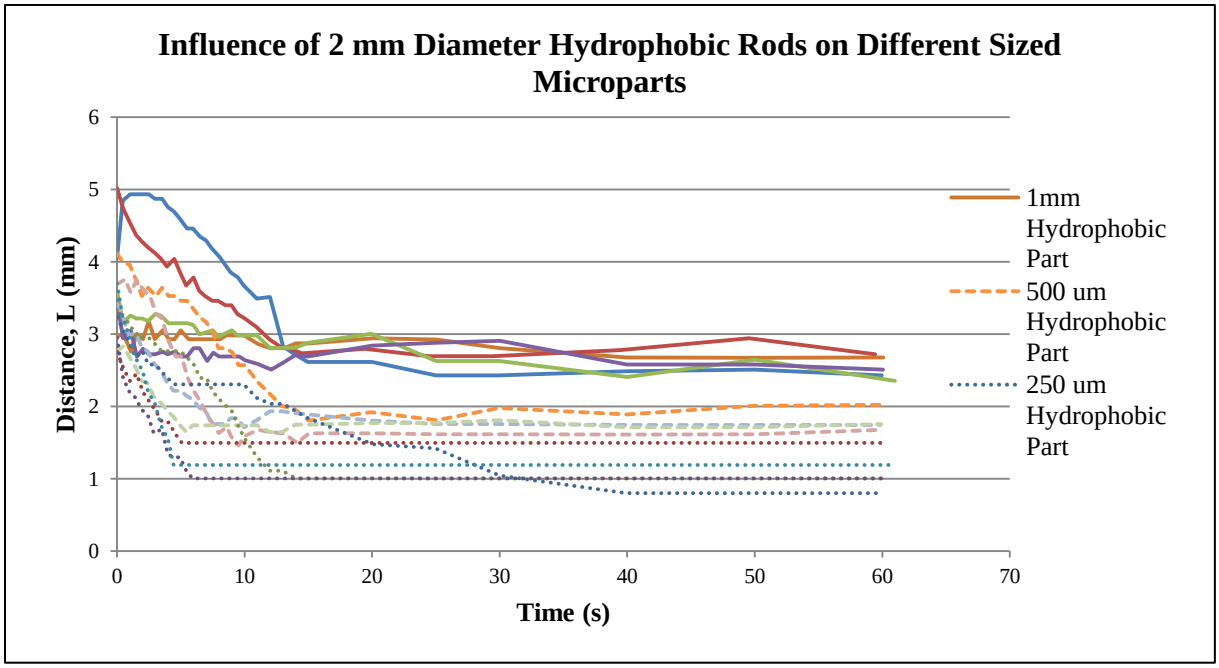

Figure 5.41: Graph of 8.5 mm rod spacing: 2 mm diameter hydrophilic rods with 1 mm, 500 µm and 250 µm parts.

In all of the trials conducted, each micropart, of all sizes, travels toward the 2 mm diameter hydrophobic rod. In each trial, the microparts orient about their z-axis to allow a leading edge to face the rod during travel. An equilibrium distance of about 2.5 mm, 1.8 mm and 1.1 mm is reached for the 1mm, 500 µm and 250 µm parts respectively. The

following picture shows a 1mm part an equilibrium distance from the 2 mm diameter hydrophobic rod.

Figure 5.42: Picture of a 1 mm part at an equilibrium distance near a 2 mm diameter hydrophobic rod.

Reasoning for the behavior of the microparts is the same as described in section 5.5.

It is concluded from the results of the sixth and seventh set of trials, outlined in sections 5.5 and 5.6, that the equilibrium separation distance that is reached is dependent upon the size of the micropart and the geometry of the interface created by the hydrophobic rods. The following table summarizes the equilibrium distances reached by the microparts in all of these trials. The average equilibrium separation distance for each set of trials is listed as well as the standard deviation, s_N, and the relative standard error, RSE for each trial set. Keeping the rod diameter constant, the equilibrium distance of the micropart increases with increasing micropart width. For a constant micropart width, the equilibrium distance increases with increasing rod diameter. Further investigation into this dependency is discussed in section 5.8.

Table 5.8: Equilibrium distance listed by trial for rod spacing of 8.5 mm.

Trial	Parameters	Equilibrium	s_N	RSE
1 mm Diameter Rods				
1	250 μm	0.78		
2	250 μm	0.86		
3	250 μm	0.78		
4	250 μm	0.65		
5	250 μm	1.20		
		Average 0.854	**0.207**	**24.3%**
1	500 μm	1.38		
2	500 μm	1.27		
3	500 μm	1.33		
4	500 μm	1.38		
5	500 μm	1.42		
		Average 1.356	**0.0577**	**4.25%**
1	1 mm	2.05		
2	1 mm	2.41		
3	1 mm	2.29		
4	1 mm	2.44		
5	1 mm	2.19		
		Average 2.276	**0.161**	**7.07%**
2 mm Diameter Rods				
1	250 μm	0.80		
2	250 μm	1.50		
3	250 μm	1.00		
4	250 μm	1.00		
5	250 μm	1.19		
		Average 1.098	**0.264**	**24%**
1	500 μm	2.02		
2	500 μm	1.74		
3	500 μm	1.61		
4	500 μm	1.75		
5	500 μm	1.67		
		Average 1.756	**0.264**	**24%**
1	1 mm	2.67		
2	1 mm	2.43		
3	1 mm	2.72		
4	1 mm	2.51		
5	1 mm	2.58		
		Average 2.582	**0.117**	**4.54%**

The figure below depicts the equilibrium distances of the different sized microparts that result from the sixth and seventh sets of trials. In each of the three sets of data shown in the bar graph, the left five bars show the equilibrium distance in trials using a 1mm diameter rod and the trials denoted by the right five bars use a 2 mm diameter rod.

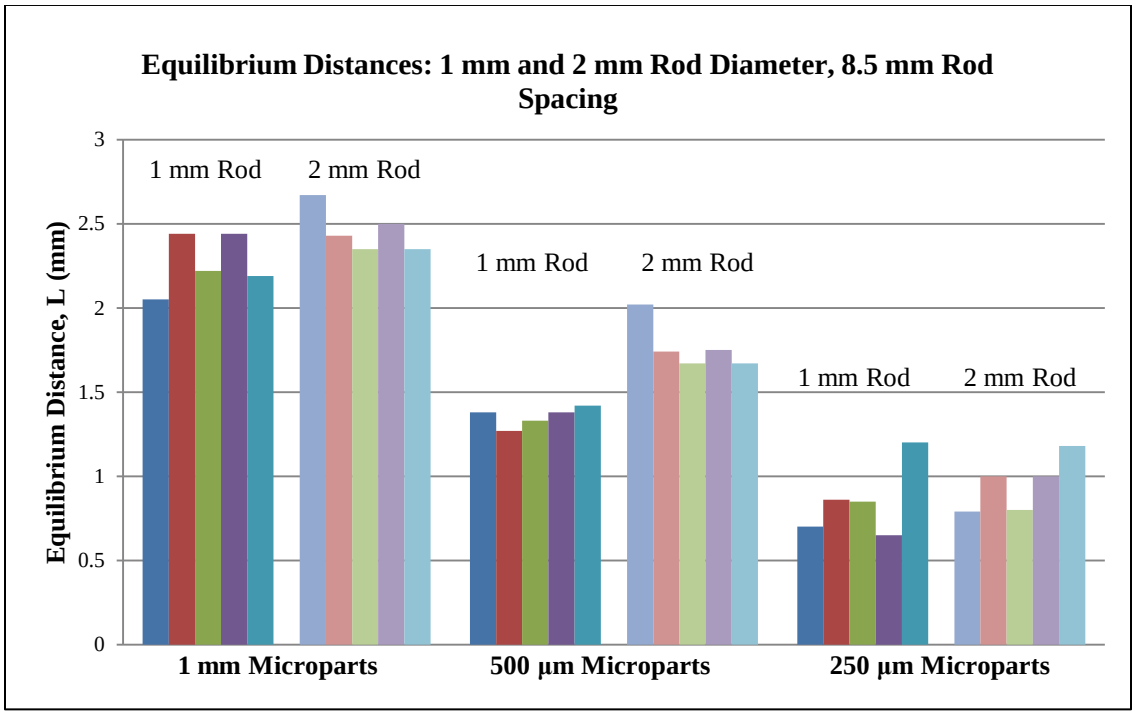

Figure 5.43: Graph of equilibrium distance: 1 mm and 2 mm rod diameters, 8.5 mm rod spacing.

5.7 Summary of Results

The results of all of the trials are compiled in Table 5.9 below for ease of reference. Each row of the table represents a subset of five trials and documents the overall trend in direction and rotational behavior of the micropart for the subset. The first seven columns outline the parameters of each subset of trials. Under the heading *Rod*, *Plate* and *Part*, the letter I or the letter O denotes whether that body is hydrophilic or hydrophobic, respectively. The *Spacing* is listed for trials where rods are used, and the

spacing given is the distance in millimeters between adjacent rods and the distance between diagonal rods, respectively. A *Rod Diameter* of 1 mm or 2 mm is listed for trials using rods. The width of the square parts is given under the heading *Part Size*. The *Placement* heading gives the location of the part at deposition, where *Diagonal* denotes placement one quarter of the length of the diagonal distance between rods, *Close* denotes placement near the rod or plate and *Away* denotes placement away from the plate. Under the heading *Overall Orientation*, the term *Edge Faces Rod* signifies that the micropart rotates during the trial until a flat edge of the micropart faces the rod as described in previous sections.

Table 5.9: Complete summary of results. I = Hydrophilic, O = Hydrophobic.

Rod	Spacing	Rod Diam	Plate	Part	Part Size	Placement	Directional Trend	Overall Orientation
I	2.1/3.38	1 mm		O	500 µm	Diagonal	None	Edge Faces Rod
O	2.1/3.38	1 mm		O	500 µm	Diagonal	Little Movement	No Trend
I	5.3/7.91	1 mm		O	500 µm	Diagonal	Away from Rod	No Trend
O	5.3/7.91	1 mm		O	500 µm	Diagonal	Little Movement	Edge Faces Rod
I	8.5/12.44	1 mm		O	500 µm	Diagonal	Away from Rod	No Trend
O	8.5/12.44	1 mm		O	500 µm	Diagonal	Toward Rod	Edge Faces Rod
I	11.7/16.79	1 mm		O	500 µm	Diagonal	Away from Rod	No Trend
O	11.7/16.79	1 mm		O	500 µm	Diagonal	Toward Rod	Edge Faces Rod
I	14.9/21.49	1 mm		O	500 µm	Diagonal	Little Movement	No Trend
O	14.9/21.49	1 mm		O	500 µm	Diagonal	Toward Rod	Edge Faces Rod
I	8.5/12.44	1 mm		I	500 µm	Diagonal	Slight Mvt Tow Rod	No Trend
O	8.5/12.44	1 mm		I	500 µm	Diagonal	Toward Rod	Edge Faces Rod
I	8.5/12.44	1 mm		O	500 µm	Close	Slight Mvt Away Rod	Edge Faces Rod
I	8.5/12.44	1 mm		I	500 µm	Close	None	No Trend
O	8.5/12.44	1 mm		O	500 µm	Close	Little Movement	Edge Faces Rod
O	8.5/12.44	1 mm		I	500 µm	Close	Little Movement	Edge Faces Rod
			I	O	500 µm	Away	None	No Rotation
			I	O	500 µm	Close	None	No Rotation
			I	I	500 µm	Away	None	No Rotation
			I	I	500 µm	Close	None	No Rotation
			O	O	500 µm	Away	All the Way to Plate	Little to No Rot
			O	O	500 µm	Close	All the Way to Plate	Little to No Rot
			O	I	500 µm	Away	All the Way to Plate	Little to No Rot
			O	I	500 µm	Close	All the Way to Plate	Little to No Rot
O	8.5/12.44	1 mm		O	1 mm	Diagonal	Toward Rod	Edge Faces Rod
O	8.5/12.44	1 mm		O	500 µm	Diagonal	Toward Rod	Edge Faces Rod
O	8.5/12.44	1 mm		O	250 µm	Diagonal	Toward Rod	Edge Faces Rod
O	8.5/12.44	2 mm		O	1 mm	Diagonal	Toward Rod	Edge Faces Rod
O	8.5/12.44	2 mm		O	500 µm	Diagonal	Toward Rod	Edge Faces Rod
O	8.5/12.44	2 mm		O	250 µm	Diagonal	Toward Rod	Edge Faces Rod

Comprehensively anaylizing the data, one can surmise that there is one major trend to draw from the entire list of trials that is the most significant. In all of the cases where the rods are treated to be hydrophobic, the rod spacing is 8.5 mm or more and the micropart is placed on the diagonal, the micropart, no matter its size, moves toward the rod and rotates until an edge faces the rod during travel. In all of these trials, the

micropart reaches an equilibrium distance away from the rod that is dependent upon the size of the micropart and the geometry of the interface created by the hydrophobic rods.

The two parameters directly influencing the equilibrium distance of the micropart are the size of the micropart and the interfacial geometry. The size of the micropart is easily described by its width. The shape of the surface may be described by calculating the curvature of the interface at separate locations along the surface. This section discusses the influence of the dimensional parameters of the micropart on the separation distance. Calculations describing the curvature along the interface is left for future work.

As previously mentioned in Chapter 2, as a fluid-fluid interface bends to accommodate the change in pressure on either side of the interface, the surface area of the interface increases. This, in turn, increases the energy in the surface at the location of increased bending. The curvature of the interface is also increased at this location. The assumption is made that the micropart avoids this area of higher energy. The additional assumption made in section 4.1.2 (that it requires more energy for the floating micropart to displace a greater amount of volume of fluid at a location of higher curvature) may also contribute to the actuation of the micropart finding an equilibrium distance. With regard to both assumptions, it is the curvature of the interface that may be directly responsible for the behavior of the micropart.

In the experimental trials, the micropart reaches an equilibrium distance at what appears to be a location on the surface just outside of where the curvature begins to dramatically increase.

An analysis of the size and mass of the silicon microparts and the equilibrium distance of the microparts aims to determine if a mathematical relationship can be made between these parameters.

Table 5.8 is expanded in Table 5.10 to include the calculated relationships of micropart mass, radius and equilibrium distance for surfaces interrupted by a 1 mm diameter rod. The micropart radius is represented as half of the micropart width and is given in millimeters. L is used to represent the equilibrium distance expressed in millimeters. The mass of the silicon microparts is given in grams and is calculated using the dimensions of the microparts and the density of silicon. Average values, standard deviations, s_N, and relative standard errors, RSE are also listed.

Table 5.10: Relationships of micropart radius and mass and equilibrium distance for rod diameter of 1 mm.

Part Width	Equilibrium Distance, *L*	*r/L*	*L*/Mass
250 μm	0.78 mm	0.1602	542608
250 μm	0.86 mm	0.1453	598260
250 μm	0.78 mm	0.1602	542608
250 μm	0.65 mm	0.1923	452173
250 μm	1.2 mm	0.1041	834782
Average	**0.854 mm**	**0.1524**	**594086**
s_N	**0.207**	**0.032**	**144387**
RSE	**24.3%**	**20.9%**	**24.3%**
500 μm	1.38 mm	0.1811	240000
500 μm	1.27 mm	0.1968	220869
500 μm	1.33 mm	0.1879	231304
500 μm	1.38 mm	0.1811	240000
500 μm	1.42 mm	0.1760	246956
Average	**1.356 mm**	**0.1846**	**235826**
s_N	**0.0577**	**0.00803**	**10035**
RSE	**4.25%**	**4.35%**	**4.25%**
1 mm	2.05 mm	0.2439	89130
1 mm	2.41 mm	0.2074	104782
1 mm	2.29 mm	0.2183	99565
1 mm	2.44 mm	0.2049	106086
1 mm	2.19 mm	0.2283	95217
Average	**2.276 mm**	**0.2205**	**98956**
s_N	**0.161**	**0.016**	**6994**
RSE	**7.07%**	**7.27%**	**7.07%**

The relationships incorporating the measured values and part parameters are discussed. When analyzing the equilibrium distances, it is found that the ratio of the average equilibrium distance, *L*, of the 1 mm part to that of the 500 μm part is 1.68 to one. Likewise, the ratio of the average equilibrium distance, *L*, of the 500 μm part to the 250 μm part is 1.58 to one. This suggests that for the sizes of the microparts tested, as the width of the micropart is increased by a factor of two, the equilibrium distance that the micropart reaches may increase by a factor of approximately 1.6.

When comparing the relationships of the ratios of part radius to equilibrium distance, *r/L*, across the different micropart sizes, a proportional relationship also emerges. The average *r/L* value of the 1 mm parts to that of the 500 μm parts is 1.19 to one. The average *r/L* value of the 500 μm parts to that of the 250 μm parts is 1.21 to one. This could signify that as the part width is increased by a factor of two, the relationship of r/L increases by a factor of about 1.2.

Comparing the relationship of the equilibrium distance to the mass of the micropart reveals that the average ratio of *L*/mass for the 250 μm parts to that of the 500 μm parts is 2.52 to one. The average ratio of *L*/mass for the 500 μm parts to that of the 1 mm parts is 2.38 to one. This could suggest that as the size of the micropart decreases by a factor of two, the relationship of *L*/mass may increase by a factor of about 2.5.

Further experimentation using more part sizes and more trials is recommended to calculate a better approximation of relationships between parameters. These approximations are based on the empirical data of the experiment and do not suggest that these correlations are absolute. Additional investigation is needed to develop a stronger theory of correlation.

An analysis of the relationship between equilibrium distance and other part parameters is carried out for the trials using a 2 mm diameter rod. The following table gives these relationships. Average values, standard deviations, s_N, and relative standard errors, RSE are also listed.

Table 5.11: Relationships between micropart radius, mass and equilibrium distance for rod diameter of 2 mm.

Part Width	Equilibrium Distance, mm	r/L	L/Mass
250 μm	0.8	0.1562	556521
250 μm	1.5	0.0833	1043478
250 μm	1	0.125	695652
250 μm	1	0.125	695652
250 μm	1.19	0.1050	827826
Average	**1.098**	**0.1189**	**763826**
s_N	**0.264**	**0.0270**	**184320**
RSE	**24.0%**	**22.7%**	**24.0%**
500 μm	2.02	0.1237	351304
500 μm	1.74	0.1436	302608
500 μm	1.68	0.1488	292173
500 μm	1.75	0.1428	304347
500 μm	1.8	0.1388	313043
Average	**1.798**	**0.1395**	**312695**
s_N	**0.157**	**0.00954**	**22821**
RSE	**8.93%**	**6.84%**	**7.30%%**
1 mm	2.67	0.1872	116086
1 mm	2.43	0.2057	105652
1 mm	2.72	0.1838	118260
1 mm	2.35	0.2127	102173
1 mm	2.51	0.1992	109130
Average	**2.536**	**0.1977**	**110260**
s_N	**0.117**	**0.0122**	**6816**
RSE	**4.54%**	**6.17%**	**6.18%**

Between the first sets of trials using rods and the seventh set of trials, as the rod diameter increases by a factor of two, the average equilibrium distance reached by the 250 μm part, the 500 μm part and the 1 mm part increases by a factor of 1.29, 1.33 and 1.14 respectively. No conclusion involving proportionality is determined from this data.

A comparison of equilibrium distances for different part sizes reveals that the ratio of the average equilibrium distance, *L*, of a 1 mm part to that of a 500 μm part is 1.41 to one and that of a 500 μm part to a 250 μm part is 1.64. This may suggest that as

part width increases by a factor of two, the equilibrium distance increases by about 1.5 for the case of a 2 mm diameter rod.

The ratio of the relationship of *r/L* of a 1 mm part to a 500 μm part is 1.42 to one and that of a 500 μm part to a 250 μm part is 1.17 to one. The ratio of the relationship of *L*/mass of a 250 μm part to a 500 μm is 2.84 to one and that of a 500 μm part to a 1 mm part is 2.44 to one. It is recommended that more trials using more parts need to be conducted in order to surmise that a proportional relationship exists between the data.

Chapter 6:

Conclusion

In this thesis, preliminary experimentation was conducted to investigate the feasibility of developing a new method for self-alignment of microparts by way of surface tension. The experiment performed analyzed the movement of silicon microparts on a hexadecane-water interface as affected by changes in interfacial geometry. To create surface deformation, both hydrophilic and hydrophobic vertical, quartz rods penetrated the interface, creating a positive or negative meniscus slope about the rods, respectively. A silicon micropart was placed on the interface away from a rod and its movement in relation to the rod was tracked.

6.1 Summary

The first set of trials tested a single, 500 μm hydrophobic micropart amidst sets of both hydrophilic and hydrophobic 1 mm diameter rods spaced in five separate spacing arrangements. It was found that for a rod spacing greater than or equal to 8.5 mm, the microparts were attracted to the hydrophobic rods and reached an average equilibrium separation distance from the outer diameter of the rod of about 1.3 mm. The 8.5 mm rod spacing produced the strongest trend and most repeatable results. The second set of trials used the 8.5 mm spacing to test hydrophilic microparts near both sets of rods. A strong attraction occurred toward the hydrophobic rods and a similar equilibrium distance was

reached. In the third set of trials, hydrophilic and hydrophobic parts were placed in closer proximity to both sets of rods to test if a similar equilibrium distance would result. The behavioral trend of the microparts was not very strong in these trials.

A fourth and fifth set of trials tested hydrophilic and hydrophobic microparts placed near and away from hydrophilic and hydrophobic flat plates to determine if an equilibrium distance would emerge. It was found that the equilibrium distance that the microparts reached in the previous trials was dependent upon the double curvature of the surface created by the rods. The flat plate did not produce an equilibrium distance.

The sixth set of trials tested 250 μm and 1mm parts away from 1 mm diameter hydrophobic rods to determine if the size of the part influenced the equilibrium distance. Results show that larger microparts reached an equilibrium position at a larger distance. The seventh and final set of trials tested all three sizes of microparts among 2 mm diameter hydrophobic rods. It was discovered that the change in the curvature of the surface caused by the larger rods created a larger equilibrium separation distance for the microparts.

A comprehensive analysis of the results reveals that a substantial trend exists in the trials utilizing hydrophobic rods. An equilibrium separation distance of the micropart was experienced in all of these trials. It is apparent that this equilibrium distance is dependent upon the size of the micropart and the curvature of the interface. For the trials performed, it was found that the equilibrium distance increased as the size of the part increased and also as the radius of the rod increased. It is noted that for the trials conducted, the equilibrium distance reached by the micropart increased by a factor of about 1.6 as the width of the micropart increased by a factor of two.

Overall, it is important to document that in all of the trials conducted using hydrophobic rods spaced 8.5 mm or more apart, the micropart *always* traveled to the rod when placed away from it. This occurred for all part sizes, whether the micropart was hydrophilic or hydrophobic, and for both rod diameters. In each of these trials, the micropart reached an equilibrium position located at a distance away from the rod. The micropart also rotated so that a flat edge faced the rod in all of these trials.

6.2 Comparison of Results to Previous Work

Velev et al. performed a study discussed in Chapter 2 where the lateral capillary immersion force between two vertical cylinders at an air-water interface was empirically measured [20]. As mentioned, when the distribution of lateral force was plotted versus the separation distance between the cylinders, the majority of the data assumed the shape of a natural logarithmic curve, decaying to zero at greater distances. For extremely small distances, though, the force values did not lie on this curve.

It is surmised that the lateral capillary forces experienced in the thesis experiment also follow a logarithmic trend. The microparts experience greater attraction or repulsion when closest to the rod and this effect decays at larger separation distances. This agrees with the results of the experiment conducted by Velev et al. Also in the thesis experiment, the microparts reach small equilibrium separation distances away from the rod. It can be concluded that at these distances, the lateral capillary forces do not follow the same behavioral pattern as they do for larger distances. Though Velev et al. use only semi-immersed bodies in their experiment, the result of this thesis is similar. In both experiments, the lateral forces are not the dominating phenomena at small separation distances.

Also discussed in Chapter 2, a review of experimental studies involving lateral capillary flotation and immersion forces was conducted by Kralchevsky and Nagayama [22]. Here, it was concluded that interface deformations created by semi-immersed bodies were caused by the wetting properties of the body. It was also concluded that deformation of the interface created the appearance of attraction and repulsion between bodies at an interface. Both of these findings are evident in the results of this thesis. The shape of the hexadecane-water interface was dependent upon whether or not the semi-immersed vertical rods were treated to be hydrophobic. This deformation was the cause of the direction of the lateral movement of the microparts.

6.3 Possible Applications

The empirical data gives evidence to suggest that the development of a self-alignment method for microparts on a fluid-fluid interface is a reasonable venture. The results show that microparts will attract to a vertical rod and remain a designated distance away from the outer diameter of the rod. It is also known that microparts that deform the interface in the same direction aggregate and form clusters [8]. Perhaps placing several microparts on an interface that attract toward a hydrophobic rod will create a ring of microparts similar to that shown in the figure below.

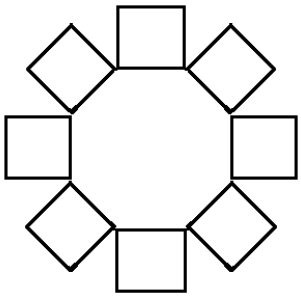

Figure 6.1: Ring of microparts formed by influence of presence of a rod.

The method of creating a ring of parts by way of interfacial surface tension may be useful in the manufacture of any mechanism where a ring of parts about a specified radius is necessary. Rods of different diameters that correlate to different equilibrium separation distances for varying interfacial curvatures and microparts can determine the dimensions of the ring formation. Once a ring of microparts is formed on an interface, there are several methods that can be used to apply the microparts to a designated area.

One possible method of efficient pick-and-place could involve the use of a circular tube that would pick up the parts via binding sites at the end of the tube. The figure below shows how a tubular fixture could be lowered around the vertical rods to pick up the microparts. The parts could then be placed elsewhere while maintaining the ringed configuration or remain on the tube.

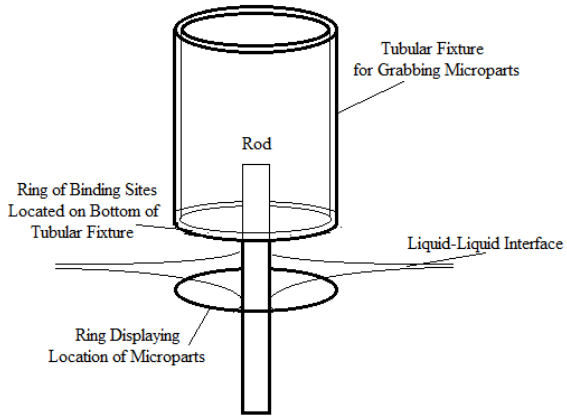

Figure 6.2: Proposed method of picking up microparts from an interface via binding sites at the end of a tubular fixture.

A second method of efficient pick-and-place involves utilizing shorter hydrophobic rods and an air-water interface. The rods would remain recessed below the top of the interface and the microparts would float higher than the top of the rod as shown in the figure below. This would allow for a flat substrate with a ring of binding sites to be

placed over the ring of microparts and lowered onto them, picking up all of the microparts simultaneously.

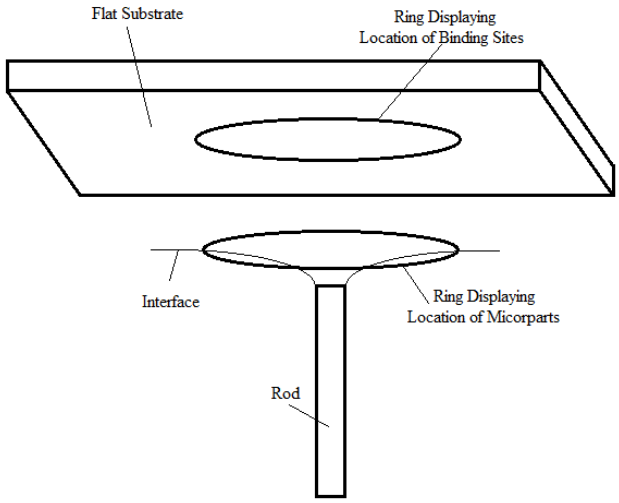

Figure 6.3: Proposed method of picking up microparts via binding sites by use of a flat substrate.

A third option for deposition of a ring of microparts onto a substrate is to slowly drain the fluid bath that microparts are floating on. Once the fluid is removed from the open container, the microparts would lie on the top of the aluminum plate, still arranged in the shape of a ring. If, instead of an aluminum plate, a substrate with binding sites is used for support of the vertical rods, the microparts could simply be lowered onto the binding sites as the fluid is drained from the container. If the surface curvature of the interface is small enough in this case to not alter the positioning of the microparts as they reach the bottom substrate, this may be a feasible method of assembly to test.

An additional application proposed for creating a ring of microparts about a rod involves the use of different shaped microparts. Utilizing microparts that are shaped to interlock when configured into a ring could be a useful method of self-alignment. The example of hexagonally shaped microparts forming a ring is pictured in the figure below.

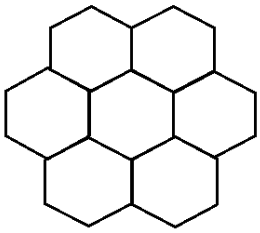

Figure 6.4: Hexagonally shaped microparts forming a ring.

In this example, as the microparts cluster about the rod, they could align so that adjacent edges "stick" to each other as aggregating bodies on an interface tend to do. It is assumed that the microparts have a high possibility of aligning in such an orientation. This inference is made based on the results of the experimental trials. In every case when the square microparts traveled to the rod, it reoriented itself so that an edge of the micropart would be facing the rod. This is described in detail in Chapter 5. Presuming that this would also be the case for the example of hexagonally shaped microparts, formation of a ring as described in Figure 6.4 is possible.

Once such a ring of microparts has taken shape, more microparts may be introduced onto the interface. It is theorized that the additional microparts may travel toward the established ring of microparts and begin to cluster about this ring, adding concentric rings of microparts. This is depicted in the figure below.

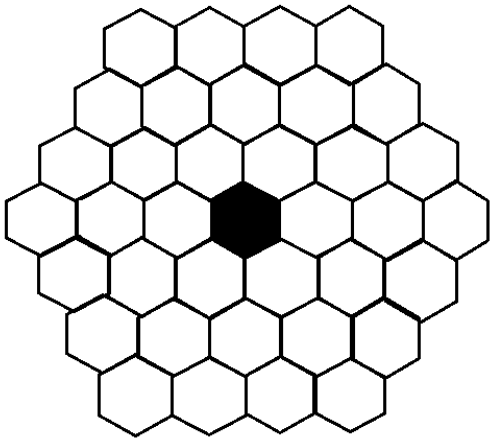

Figure 6.5: Three concentric rings of hexagonally shaped microparts. The shaded center represents a hole where a vertical rod would be located and no micropart is present.

This may occur until an entire sheet of microparts forms about a rod. The first ring created about the rod would serve as a catalyst for the creation of the entire sheet.

A direct application of a sheet of silicon microparts is the manufacture of photovoltaic cells as silicon wafers are currently the dominating technology used in photovoltaic construction [8].

6.4 Future Work

Additional testing is necessary for further understanding of the relationship between equilibrium separation distance, interfacial curvature and micropart dimensions. Continuing experiments would include introducing several different sized microparts and microparts of different shapes deposited at different locations on the interface. More tests could also study the effects of different levels of hydrophobicity of the rods. Different contact angles between the rod surface and the interface could be studied to determine an influence on an equilibrium separation distance.

Further numerical analysis would involve developing an accurate description of the interface by deriving an equation of the shape of the interfacial plane. In doing so, calculation of the curvature of the interface along different locations could help reveal a relationship between the geometry of the interface and an equilibrium separation distance.

Completion of the Surface Evolver model is recommended for evaluation of lateral capillary forces along the interface and energies inherent in the system. Understanding such values may assist in further discoveries of relationships involving equilibrium separation distances from the rods.

List of References

[1] Kralchevsky, P., Nagayama, K., 2001, *Particles a Fluid Interfaces and Membranes: Attachment of Colloid Particles and Proteins to Interfaces and Formation of Two-Dimensional Arrays*, Elsevier, Amsterdam.

[2] Sato, K., Ito, K., Hata, S., Shiokohbe, A., 2003, "Self-alignment of microparts using liquid surface tension-behavior of micropart and alignment characteristics," *Precision Engineering*, 27:42-50.

[3] Dalin, J., Wilde, J., Zulfiqar, A., Lazarou, P., Synodinos, A., Aspragathos, N., 2010, "Electrostatic attraction and surface-tension forces for accurate self-assembly of microparts," *Microelectronic Engineering* 87:159-62.

[4] Sivagnanam, V., Sayah, A., Gijs, M., 2008, "Bead-based single protein micro-array realized through electrostatic self-assembly of carboxylated beads," *Microelectronic Engineering*, 85:1355-8.

[5] Horenstein, M., 2009, "Electrostatics and nanoparticles: what's the same, what's different?" *Journal of Electrostatics* 67:384-93.

[6] Leunissen, M., Zwanikken, J., van Roij, R., Chaikin, P., 2007, "Partitioning at the oil-water interface as a source of tunable electrostatic effects in emulsions with colloids," *Physical Chemistry Chemical Physics*, DOI: 10.1039/b711300e.

[7] Aubry, N., Singh, P., 2008, "Physics underlying self-assembly of micro- and nano-particles at a two fluid interface using an electric field," *Physical Review E*, 77, 056302.

[8] Cruz-Campa, J.L. (Sandia Nat. Labs., Albuquerque, NM, United States); 2011, "Microsystems enabled photovoltaics: 14.9% efficient 14 μmm thick crystalline silicon solar cell," *Solar Energy Materials and Solar Cells*, 95:2:551-8.

[9] Whitesides, G., Grzybowski, B., 2002, "Self-assembly at all scales," *Supramolecular Chemistry and Self-Assembly*, 295:2418-21.

[10] Zhou, S., 2002. "On forces in microelectromechanical systems," *International Journal of Engineering Science*, 41:313-35.

[11] Whitesides, G., Boncheva, M., 2002, "Beyond molecules: self-assembly of mesoscopic and macroscopic components," *Proceedings of the National Academy of Sciences of the United States of America*, 99:8:4769-74.

[12] Syms, R., Bright, V., 2003, "Surface tension-powered self-assembly of microstructures-the state-of-the-art," *Journal of Microelectromechanical Systems*, 12:4:387-417.

[13] Song, S., Pan, L., Li, Y., Pu, L., Zhang, R., Zheng, Y., 2008, "Assembly of polyaniline: mechanism study,"*Journal of Chemical Physics*, 2:2:187-92.

[14] Basore, P., Gee, J., 1994, "Crystalline-silicon photovoltaics: necessary and sufficient," *Institute of Electrical and Electronics Engineers*, 2:2254-7.

[15] White, F., 2008, *Fluid Mechanics, 6th ed.*, McGraw-Hill, New York, USA.

[16] Kralchevsky, P., Nagayama, K., 2000, "Capillary interactions between particles bound to interfaces, liquid films and biomembranes," *Advances in Colloid and Interface Science*, 8:2-3:145-92.

[17] Nicolson, M. M, 1949, "The interaction between floating particles," *Mathematical Proceedings of the Cambridge Philosophical Society*, 45:2:288-95.

[18] Chen, P., Susna, S., Newman, A., 1999, "Thermodynamics of liquid films and film tension measurements," *International Journal of Mineral Processing*, 56:75-97.

[19] Tsai, C., Hsieh, C., Yeh, A., 2007, "Self-alignment of microchips using surface tension and solid edge," *Sensors and Actuators A*, 139:343-9.

[20] Velev, O., Denkov, N., Paunov, V., Kralchevsky, P., Nagayama, K., 1993, "Direct measurement of lateral capillary forces," *Langmuir*, 9:3702-9.

[21] Velev, O., Denkov, N., Paunov, V., Kralchevsky, P., Nagayama, K., 1994, "Capillary image forces II: experiment," *Journal of Colloid and Interface Science* 167:66-73.

[22] Kralchevsky, P., N., Paunov, Denkov, N., Nagayama, K., 1994, "Capillary image forces I: theory," *Journal of Colloid and Interface Science*, 167:47-65.

[23] Brakke, K., 2008, "Surface Evolver Manual," *The Surface Evolver Version 2.30*, Susquehanna University, 4 January 2011, http://www.susqu.edu/brakke/evolver/evolver.html

[24] Brakke, K. 2008, "Surface Evolver Workshop," *The Surface Evolver Version 2.30*, Susquehanna University, 4 January 2011, http://www.susqu.edu/brakke/evolver/workshop/workshop.htm

[25] Shea, T. M., “Durable hydrophobic surface coatings using silicone resins,” US Patent Application # 7344783 B2, description 4.